ACTUATION FATIGUE OF SHAPE MEMORY ALLOYS

A Thesis

by

CHRISTOPHER ALLEN CALHOUN

Submitted to the Office of Graduate Studies of
Texas A&M University
in partial fulfillment of the requirements for the degree of

MASTER OF SCIENCE

May 2012

Major Subject: Aerospace Engineering

ACTUATION FATIGUE OF SHAPE MEMORY ALLOYS

A Thesis

by

CHRISTOPHER ALLEN CALHOUN

Submitted to the Office of Graduate Studies of
Texas A&M University
in partial fulfillment of the requirements for the degree of

MASTER OF SCIENCE

Approved by:

Chair of Committee,	Dimitris C Lagoudas
Committee Members,	Gary Fry
	Vikram Kinra
Head of Department,	Dimitris C Lagoudas

May 2012

Major Subject: Aerospace Engineering

ABSTRACT

Actuation Fatigue of Shape Memory Alloys. (May 2012)
Christopher Allen Calhoun, B.S., Virginia Polytechnic Institute and State University
Chair of Advisory Committee: Dr. Dimitris C. Lagoudas

A testing method was developed to cycle quickly and repeatably Ni60Ti40 (wt. %) SMA specimens through temperature-induced transformation while under constant stress until failure. Previous works have shown fatigue cracks to initiate in or around Ni_3Ti precipitates during repeated thermal cycling in this highly Ni-rich alloy. Actuation fatigue tests were conducted on specimens produced from material from different material suppliers and direction relative to cold-rolling. The specimens were placed under a constant applied stress of 200 MPa and thermally cycled through complete transformation. Some of the specimens were homogenized for 1 hour in a vacuum furnace and the rest were homogenized for 2 hours in a nitrogen furnace, and were all aged for 20 hours.

It was seen during actuation fatigue testing that specimens homogenized for two hours had higher actuation strain, accumulated more irrecoverable strain and had longer actuation fatigue lives compared to specimens homogenized for one hour. Another trend observed was that specimens with the greatest amount of accumulated irrecoverable strain, which was caused predominately by transformation induced plasticity, had the longest actuation fatigue lives. Postmortem analysis showed a change in cracking behavior with precipitate orientation. Cracks initiated inside the Ni_3Ti precipitates oriented parallel to the loading direction and at the interface between the precipitate and matrix when perpendicular. Two dimensional plane stress finite element simulations of a linear elastic ellipsoidal precipitate inside a non-linear transforming SMA matrix were conducted to explain further the change in cracking

behavior by analyzing the stress fields in and around the precipitates. The results showed the stress inside the precipitate was greater when oriented parallel than perpendicular to the loading direction, which explains the observed change in cracking behavior.

Another objective of actuation fatigue testing is to generate useful data to create predictive tools for future SMA actuator designs. A work-based method has been developed using actuation fatigue results found in literature. The method is shown to fit accurately data found in literature to a curve with only two material parameters. The results of this method show promise to predict accurately the actuation fatigue life of SMA components, however more testing is necessary to validate completely the method.

To my grandparents, Henry and May Katharine

ACKNOWLEDGMENTS

The first acknowledgement is to the Creator for the beautifully complex world He has made for us. This thesis would not be possible without the loving support of my Family, especially Mom, Dadio, Brotherman, Grandma and Grandpa. My entire family has supported me through my entire academic career, and continue to provide unwavering support through all my triumphs and struggles. My family alone did not provide all the support necessary; my good friends deserve much credit, especially Dara.

Professionally, I would like to acknowledge Dr. Dimitris Lagoudas for giving me the opportunity to work on this project. His patience and support through this work are greatly appreciated and will serve as a life long lesson on mentoring. Dr. Darren Hartl and Dr. Parikshit Kumar have provided much guidance through my work at Texas A&M. None of this work would have been possible without Jim Mabe at The Boeing Company providing the funds and experience to conduct such a project. Dr. Norman Dowling at Virginia Tech also deserves much credit for getting me interested in metal fatigue and material testing as well as teaching me the importance of attention to detail in experimentation. I would also like to acknowledge Justin Schick for teaching me about fatigue of SMAs and serving as a mentor as I adjusted to work in the SMART group. The rest of the SMARTans deserve much credit, especially my co-worker, roommate, and friend Brian Lester, and my friend and officemate, Stephen Oehler. Without Brian, it is hard to say what my life would be like. Without Stephen, I would not have someone to share my excitement at work, Fridays would be just another day of the week and late night rants would go unheard. My roommate and friend, Brent Macomber, also deserves and acknowledgement for being a good supportive friend throughout my time at Texas A&M.

Finally, I would like to acknowledge the 33 students and faculty who lost their lives during the shooting on April 16, 2007 at Virginia Tech, especially Dr. Librescu. Dr. Librescu's dedication and sacrifice will forever motivate me to try to be the great teacher and researcher he was.

TABLE OF CONTENTS

LIST OF TABLES

LIST OF FIGURES

FIGURE Page

FIGURE Page

CHAPTER I

INTRODUCTION

Shape Memory Alloys (SMAs) have been studied for multiple decades by many researchers with significant published works starting in 1961 by Buehler and coworkers from the Naval Ordinance Laboratory [1]. SMAs are unique metals capable of undergoing repeated solid-solid phase transformations at relatively low temperatures between an austenitic and martensitic phase, which can result in large recoverable inelastic strains. The unique thermo-mechanical response has made SMAs useful for a wide range of engineering applications, most notably in the biomedical, automotive and aerospace industries. SMAs are used in cardiovascular stents, orthodontic braces, and dental drills in the biomedical field [2, 3, 4]. These applications usually take advantage of the pseudoelastic phenomena of SMAs, also known as superelasticity. SMAs undergo stress-induced transformation from the austenitic to martensitic phase upon loading, and upon unloading transform back into the austenitic phase under pseudoelastic loading.

In the automotive and aerospace industries, SMAs are being utilized as actuating materials in actuators with high energy densities [5, 6, 7, 8, 9, 10]. SMAs undergo temperature-induced transformation while under an applied stress when used as an actuating material, resulting in large recoverable strains. SMAs have been studied in a wide range of applications in the automotive industry, and in the aerospace industry, engineers at The Boeing Company have utilized SMAs in a variety of applications [5, 6, 9, 10]. One example is the successfully designed, built and flight tested Variable Geometry Chevron (VGC), which utilizes SMAs to morph the shape of the chevrons

---

The journal model is International Journal of Engineering Science.

on the aft side of the fan cowling on the engine of a Boeing 777 to change its noise and efficiency characteristics. This allows for a quiet configuration for take-off/landing, and a more efficient, though noisier, configuration while the plane is at cruising altitude [9]. A similar application, also developed at The Boeing Company, was the Variable Area Fan Nozzle [10]. This application changed the noise and efficiency characteristics of an engine by changing the geometry of the exhaust flow structure by using SMAs to deflect the aerostructure like the VGC.

SMAs show great potential, however, reliability and durability of SMAs needs to be understood before commercial use. One key aspect in determining their reliability is understanding effects of repeated transformation on thermo-mechanical response and integrity of SMAs. Most industries have regulatory agencies to ensure the safety of new products. The FDA has strict requirements on the fatigue performance in the biomedical industry, and the FAA requires repeatable and safe operation of actuators for implementation on an airplane in the aerospace industry. Many studies focused on effects of repeated transformation and are categorized by loading path, either pseudoelastic or actuation, and phenomena being studied, either fatigue life or evolution of material response. Evolution of the material response, termed functional fatigue, has been studied by a variety of researchers, and is a critical consideration for design of new SMA applications [11, 12, 13, 14]. Study of transformation-induced fatigue life is commonly referred to as structural fatigue. Many works have shown structural fatigue of SMAs, most of which have focused on pseudoelastic loading paths. Most studies on structural fatigue have focused on understanding the fundamental material fatigue response, but few studies have focused on component durability testing [15]. Understanding fundamental material response provides insight into failure mechanisms for future alloy development, as well as generate necessary data to develop a life prediction method to be used in future design processes.

A. Literature Review

1. Transformation-induced Fatigue

Fatigue behavior of SMAs was not studied until many years after SMAs had been developed. The first study on fatigue behavior of SMAs was published in 1978 by Delaey and co-workers in which CuZnAl specimens were put under cyclic stress until failure [16]. This was similar to the stress-based fatigue testing being done on conventional metals at the time. Around the same time, Melton and Mercier conducted similar experiments on a slightly different CuZnAl alloy in 1979 [17]. In 1979, Melton and Mercier also conducted some of the first work on fatigue behavior of NiTi SMAs [18]. Fatigue crack growth and pseudoelastic fatigue experiments were conducted on NiTi wire specimens where the fatigue crack growth rates were comparable with conventional metals. Fatigue life for a specimen tested with a strain amplitude of 5% had a fatigue life of 1,000 cycles, which is much greater than typically observed 1% strain amplitude for 1,000 cycles until failure in conventional metals [19].

Many additional researchers studied transformation-induced fatigue behavior of these unique materials, mainly focusing on pseudoelastic fatigue, as the development of SMAs, particularly NiTi alloys, showed more promise in engineering applications. A rotating-bending apparatus has been commonly used to cycle specimens until failure in most pseudoelastic fatigue studies [20, 21, 22, 23, 24, 25]. An SMA wire is bent into a desired radius, and the wire is rotated in a rotating-bending experiment, resulting in a constant-amplitude cyclic strain. This testing method is not widely used in conventional metals, but serves as a way to apply large strain amplitudes quickly and consistently to SMA wires at a cycling rate of 100-1000 c.p.m. [23].

Along with the continued study of structural fatigue from these early experiments, there were more recent studies on fatigue crack growth rates in SMAs. McK-

elvey and Ritchie (2001) conducted experiments to determine ultimate strength and crack growth behavior of NiTi SMAs in different phases [26]. Uniaxial tensions tests were conducted to determine ultimate strength of the alloy tested as 4 different temperatures; stable austenite (120^o C), pseudoelastic austenite (37^o C), and two in martensite (-65^o C and -177^o C). Compact tension specimens were cyclicly loaded at all four temperatures, and crack length was monitored to study fatigue crack growth rates. Pseudoelastic austenite specimens had the fastest crack growth rates of the four temperatures studied, followed by stable austenite, and martensite cases had the slowest crack growth rates. Crack growth rate in both initially austenitic cases, were strongly dependent on peak stress intensity factors and the change in the stress intensity factors during the cyclic loading. Typically, ductile materials have a stronger dependence on the change in intensity factor, and brittle materials have a strong on the peak stress level, so these tests indicate that SMAs respond as a transition between ductile and brittle materials.

2. Actuation Fatigue of SMAs

There have been many studies focusing on the structural fatigue of SMAs undergoing pseudoelastic cycling under constant temperature, while only a limited number of studies have considered thermal cycling. One of the earliest studies on structural fatigue of SMAs undergoing thermal cycling was conducted by McNichols and Brookes (1981), which was motivated by potential heat engine applications [27]. SMA wires were heat set in a helical shape, and thermo-mechanically cycled until failure. Results were compared with previous work of Mercier and Melton (1979), in which SMA wire was pseudoelastically cycled [28]. It was shown that the correlation between the strain amplitude and fatigue life was consistent for both loading paths. There were two key conclusions from this work: first, a linear log-log relationship between strain

amplitude and the fatigue life exists under these loading conditions, and second NiTi can undergo strains an order of magnitude larger for a given number of cycles to failure when compared to conventional metals. While this work considered thermal cycling, the specimens still underwent repeated stress-induced transformation.

The first study conducted on fatigue of SMAs undergoing repeated temperature-induced transformation was done by Bigeon and Morin (1996) [29]. NiTiCu and CuZnAl wire specimens were thermally cycled through transformation under a constant applied stress until failure while in a silicon oil bath. Initially, the temperature of the liquid bath was cycled to induce transformation, which proved to be time consuming. Specimens were placed in chilled silicon oil maintained below the martensitic finish temperature to increase cycling rates while an electric current was applied to heat specimens into the austenitic phase, and removed to allow forced convection to cool specimens back into the martensite phase. Applied stress used for these experiments ranged from 50 to 800 MPa for the NiTiCu specimen, and from 20 to 200 MPa for the CuZnAl specimens. A correlation between the applied stress and actuation fatigue life was observed for each material system. The authors concluded that a modified version of the Wohler model for life prediction was sufficient for actuation fatigue, in which the applied stress is correlated with fatigue life rather than stress amplitude used in conventional fatigue. It is important to note that only complete actuation, or when the specimens were cycled between a completely austenitic phase and completely martensitic phase, was considered for this testing.

More recent efforts at Texas A&M have focused on actuation fatigue of NiTiCu and NiTi SMAs. In the first work at Texas A&M, Miller and co-workers thermally cycled NiTiCu wire specimens through complete and partial transformation while under constant stress [30, 31]. Specimens were placed in a circulating ethylene-glycol environment maintained below the martensitic finish temperature. Specimens were

heated by applying a DC current, and cooled by removing the current to allow forced convection. One main objective of this testing was to observe effects of heat treatment on actuation fatigue life. As such, specimens with different heat treatments were cycled through complete actuation. Another objective of this work was to observe the effect of partial transformation on the actuation fatigue life. All specimens underwent the same heat treatment for this phase of testing. Two stress levels were used, and ten specimens were tested at each stress level with varying levels of actuation strain. Amount of actuation was controlled by adjusting the heating and cooling time of the specimens. Actuation fatigue life was shown to have a strong correlation with applied stress level under thermal cycling when amount of actuation is kept constant, as was seen by Bigeon and Morin (1996) [29]. Analysis of partial transformation showed a correlation between the actuation strain amplitude and actuation fatigue life for each applied stress. A correlation between accumulated irrecoverable strain at failure and actuation fatigue life was observed, and fit to a reformulated version of the Mason-Coffin Law. Typically, the Manson-Coffin relation is used between the plastic strain accumulation rate (per cycle), and fatigue life, where as Lagoudas et. al (2009) compared total irrecoverable strain and fatigue life [31].

Bertacchini and coworkers analyzed the effects of corrosion on the fatigue life of SMA wires made of the same NiTiCu composition used by Lagoudas et. al (2009) but with a slightly different heat treatment in a follow up study [31, 32, 33]. NiTiCu wire specimens were placed in a chilled ethylene-glycol solution while under constant stress, and thermally cycled. The specimens were heated by applying direct electrical current running through the specimen, and cooled through forced convention. Tests where conducted at full and partial actuation strain, which was defined as cycling from 25% and 75% of full actuation. The combination of current and the ethylene-glycol solution caused corrosion on the specimen surface as a brittle oxide layer formed on

the specimen, and cracks formed due to the incompatibility of the thermo-mechanical response of the non-transforming oxide layer and transforming core of the wire. Results showed a strong correlation between irrecoverable strain at failure and actuation fatigue life as was observed by Lagoudas et. al (2009).

Schick (2009) conducted the first study of the actuation fatigue of specimens produced from plate material at Texas A&M [34]. In this work, flat-sheet fatigue specimens were machined from Ni60Ti40 (wt. %) plate using electro-discharge machining (EDM), which left a recast layer on the surface of the specimens. This material has been shown to be an effective actuating material in the VGC, and is why it was chosen for this study [9]. This material is known for its high volume fraction of Ni-rich precipitates, namely Ni_3Ti and Ni_4Ti_3, which improve the dimensional stability of this alloy. The specimens were thermally cycled through complete transformation while under constant applied stress. Resistive Joule heating was applied and removed while the specimens were in a chilled environment to thermally cycle specimens as was done in previous studies. Three different circulating fluid environments were utilized, which were ethylene-glycol solution, gaseous nitrogen and chilled air. The testing apparatus that had an ethylene-glycol solution environment was the same testing set-up used in Bertachinni et. al (2009) [33]. A new test apparatus was built which had a gaseous nitrogen test environment, which was chilled by injecting liquid nitrogen into the testing environment. The liquid nitrogen would evaporate and chill the test chamber to below freezing temperatures. Using gaseous nitrogen proved to be expensive and time consuming to maintain, so the chilled air environment was developed. Dry, filtered, and compressed air was run through a vortex tubes, which injected the test chamber with a continuous stream of chilled air. Results showed that the recast layer left by the machining process shortened actuation fatigue life. It was also seen that the ethylene-glycol environment combined with resistive heating

was corrosive and in turn shortened actuation fatigue life of specimens. Experiments in which specimens were in gaseous nitrogen and chilled air environments resulted in comparable fatigue lives, with no indication of corrosion. It was observed that cracks initiated in or around the location of Ni_3Ti precipitates, which is likely caused by incompatibility of the thermo-mechanical response between a non-transforming precipitate and transforming matrix, from postmortem analysis. Another observation from the work of Schick, was large amount of scatter in fatigue life results, which could be caused by the size of the specimens [34].

In the work of Ramaiah et. al (2009), actuation fatigue tests were conducted on NiTi wire specimens [35]. Specimens were placed under constant stress, and thermally cycled using resistive heating achieve transformation into the austenitic phase and removed to allow convection to cool specimens back into the martensitic phase. This study focused on the cracking behavior in the SMA wires. It was observed that there was periodic cylindrical cracking, similar to that observed by Bertachinni (2009), but without a corrosion layer [33]. It was concluded that cracks initiated in the center of the wires undergoing actuation cycling, however, there was no preferred crack initiation location in isothermal fatigue tests. This is believed to be caused by thermal gradients that are present in actuation loading and not in isothermal tests. It was also concluded that combination of cracks and resistive heating can cause large thermal gradients accelerating the growth of cracks, despite what had been previously observed by Bigeon and Morin (1996) [29].

B. Outline and Objectives

Actuation fatigue tests were conducted on Ni60Ti40 (wt. %) in a follow up effort to Schick (2009) [34]. The prior study by Schick (2009) showed large scatter in fatigue

life, so new testing frames were built to thermo-mechanically cycle larger specimens in an effort to reduce the scatter in the actuation fatigue life [34]. Specimens were placed under constant stress while in a circulating chilled air environment. An AC current was passed through the specimens to heat into the austenitic phase, and removed to allow the specimens to cool into the martensitic phase. The geometric ratios on the specimens were kept constant, but with dimensions doubled, resulting in specimens that were 50-100 grains thick. Schick (2009) also showed cracking to initiate in or around Ni_3Ti precipitates. Tests were conducted with varying orientations of precipitates relative to loading to further understand effects of precipitate orientation. Two different heat treatments were used on the specimens, to see the effect of homogenization time on the actuation fatigue response.

In Chapter II, the testing method is presented. The chapter begins with the design and explanation of the testing apparatus. The specimen geometry is also presented, with justification of the selection process. The testing method was verified using infrared imaging, and results are shown. A complete specimen list is presented, and details heat treatment and origin of all specimens. Chapter II concludes with a microstructural description of each of specimen groups. Optical micrographs were used to characterize the specimens into three groups, which where uniformly parallel, parallel with variation and perpendicular with variation, based on the orientation of the Ni_3Ti precipitates relative to the loading direction.

In Chapter III, the results from the testing described in the previous chapter are presented. Accumulation of irrecoverable strain is shown to drastically effect the actuation fatigue life. It was observed that irrecoverable strain was greatest in specimens with longest fatigue lives, and lowest in specimens with shortest fatigue lives. The specimens which had two hours of homogenization heat treatment at 850^o C had longer fatigue lives, with higher actuations strain and amount of irrecover-

able strain. It was also seen that the actuation fatigue life was dependent on the precipitate orientation. The results showed that specimens with precipitates oriented uniformly parallel to the loading direction underwent the greatest number of cycles to failure, and specimens with precipitates perpendicular with variation underwent the fewest. Postmortem analysis showed a change in cracking behavior with the precipitate orientations. Cracking initiated inside the Ni_3Ti precipitates oriented parallel to loading and at the interface between the transforming matrix and precipitates oriented perpendicular to loading.

Numerical simulations of an elastic precipitate inside a transforming matrix were conducted to further explain the change in cracking behavior. A two dimensional unit cell was developed with four Ni_3Ti precipitates uniformly distributed, and utilizing symmetry of the unit cell a boundary value problem was defined to reflect the loading of the actuation fatigue specimens. The plane stress boundary value problem solved is described in detail in Chapter IV. Results showed that the Von Mises stress inside precipitates is much greater when precipitates are oriented parallel to loading.

A life prediction method is developed for actuation fatigue in Chapter V. Using results of previous studies, Schick (2009), Lagoudas et. al (2009) and Bertacchinni et. al (2009) the method is verified [31, 33, 34]. Results presented in Lagoudas et. al (2009) is used to show that the work-based method reduces to a strain-based method for experiments with one applied stress level [31]. Results presented in Bertacchinni et. al (2009) is used to show that the work-based method reduces to the Wohler model used in Bigeon and Morin (1996) in experiments with one actuation strain level [33, 29]. Trial predictions are also conducted using results presented in Lagoudas et. al (2009) [31]. Actuation fatigue test results from one stress level with different levels of actuation are used to predict tests conducted at another stress level.

The conclusions from this work are presented, along with some proposed future

work in Chapter VI.

CHAPTER II

ACTUATION FATIGUE TEST METHOD

The current test method was developed as a continuation of previous works at Texas A&M University [31, 30, 32, 33, 34]. Two prior studies, Bertacchinni et. al (2009) and Miller (2000) developed methods for thermally cycling wire specimens through transformation while under constant stress until failure [30, 33]. In a follow up study by Schick (2009), the testing method was expanded to incorporate flat sheet fatigue specimens that were larger than previously studied SMA wires [34]. Small specimen size, as specimens were only 25-50 grains thick, resulted in significant scatter was seen in fatigue life data. To this end, a testing method was developed to thermally cycle larger specimens through complete transformation.

Specimens were placed under constant stress in a chilled air environment in the current study, while Joule heating was applied to heat the specimens above austenitic finish temperature, and removed to allow the specimen to cool below martensitic finish temperature. Specimens were cycled until complete rupture. A schematic of the desired load path drawn on a phase diagram and the corresponding strain-temperature response are shown in Fig. 1. Specimens were held under constant stress through temperature-induced transformation to be consistent with previous works and to avoid added complexities of testing. Though, SMAs undergo a varying stress through temperature-induced transformation in many actuator applications.

A. Specimens

The specimen geometry was chosen based of Schick (2009), which was the first actuation fatigue tests [34]. The specimen geometry presented in Schick (2009) and the current work is similar to commonly used flat-sheet fatigue specimens from conven-

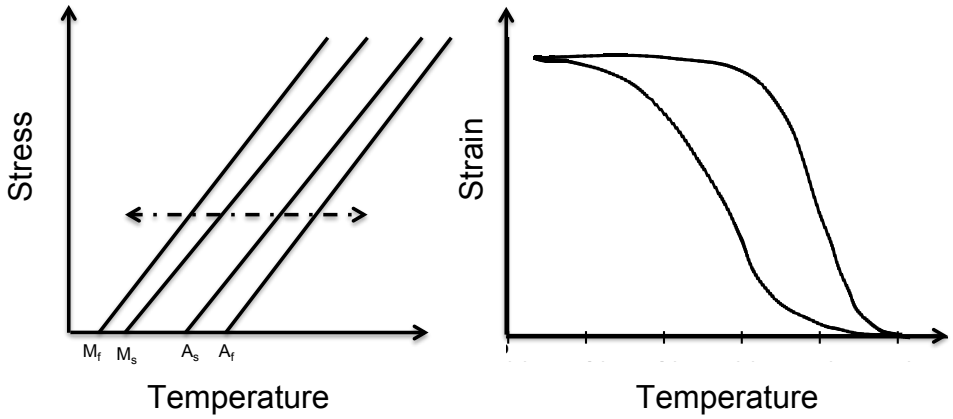

Fig. 1. Schematic of actuation fatigue loading on the phase diagram, shown by dashed line

tional fatigue experiments, which is described in ASTM standard E606-04 with elongated gauge to increase accuracy of strain measurements, and reduced cross-sectional area to accelerate cycling rates [36]. Specimens were produced using electro-discharge machining (EDM). All specimens were heat treated, polished and tested.

1. Specimen Geometry

Flat-sheet fatigue specimens with the cross section of 0.51 mm by 1.01 mm were tested in the work of Schick (2009) and large scatter was observed in fatigue life data [34]. One possible explanation is size of specimens, as specimen thickness was only between 25 and 50 times grain size. For the current study, the same specimen geometry was chosen, but with all dimensions approximately doubled resulting in a cross section of 1 mm by 2.1 mm. Specimens were 50-100 grains thick and 100-200 grains wide along the test gauge. Fig. 2 shows a specimen drawing with dimensions.

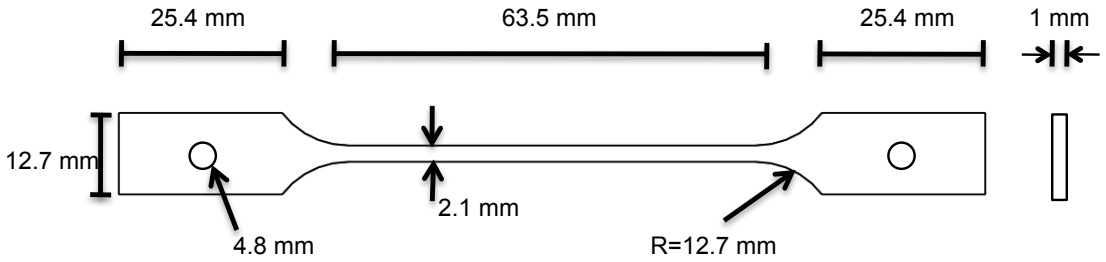

Fig. 2. Flat sheet fatigue specimen dimensions used in current study

2. Specimen Preparation

Specimens were produced from quarter or half inch thick cold-rolled Ni60Ti40 (wt. %) plate using EDM, which left a recast layer on the surface of the the specimens. Internal stresses in raw material was removed by heating the raw material to 850^o C in an air furnace and cooled in the furnace prior to machining. Material can shift during cutting and result in misshaped specimens, without removing internal stresses. The profile of the specimen was then cut out of plates, then specimens were cut to desired thickness. Upon completion of machining, specimens were heat treated, which was comprised of a homogenization and aging treatment. After heat treatment, the recast layer left by EDM was then removed using rotary grinding. The recast layer on the thinnest sides of the specimens, was removed using a 3/8 inch aluminum oxide grinding stone on a variable speed Dremmel. Sides were then polished using a 3/32 inch, 400-grit rubber polishing bob. Specimens were put into a holder to prevent any bending of specimens during preparation of thin sides while each side of the specimen was run along grinding/polishing heads with little force normal to the faces. An image of specimen polishing holder is shown in Fig. 3. A continuous spray of water was applied during polishing and grinding of sides to prevent specimens from heating.

Specimens were mounted into a custom built specimen holder to grind and polish the widest faces. The recast layer was ground off using a wet grinding wheel,

Fig. 3. Image of a specimen in the holder used to polish the thinnest sides of the specimen

starting with 400 grit grinding paper then 1200 grit, and finally 2000 grit. An image a specimen holder used to hold the specimen flat during grinding and polishing of the widest sides is shown in Fig. 4. The specimens were held in the holder using

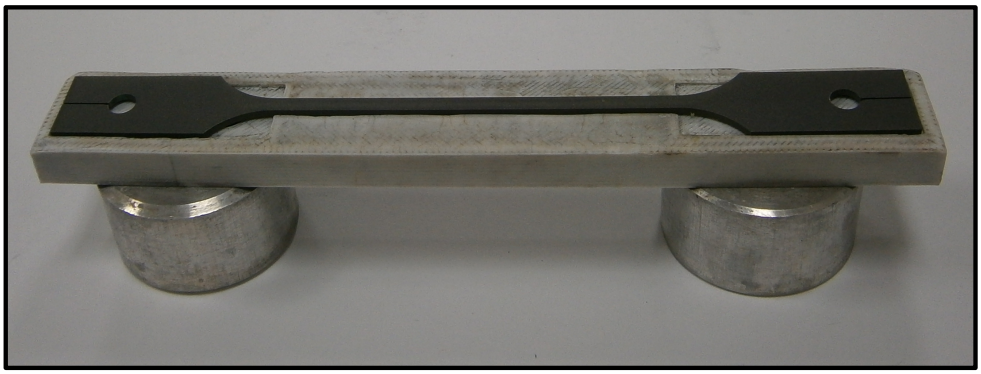

Fig. 4. Image of an unpolished specimen in the holder used to hold specimen flat during grinding and polishing of widest faces

double sided tape, which was removed after polishing using denatured alcohol. After the grinding was completed, the surfaces were polished using a polishing disk and solution. The polishing solution was initially a suspension of 5 μm aluminum oxide particles, followed by a suspension of 0.3 μm aluminum oxide particles for roughly four minutes per solution and face. All specimens had a mirror finish on widest sides upon completion. Grinding and polishing removed the recast layer as well as the heat

affected zone left by EDM, resulting in the removal of at least 70 μm from each side, and surface scratches that would shorten the actuation fatigue life. Micrographs were taken of the surface finish to verify there were no cracks, scratches or remnants of the recast layer and to observe the Ni_3Ti precipitates after the specimens were polished.

B. Test Apparatuses

Four actuation fatigue apparatuses were constructed to quickly and repeatedly cycle specimens through temperature-induced transformation for the current testing. Test apparatuses were similar to those used by Schick (2009), with some modifications that were necessary to account for the increased specimen dimensions [34]. Specimens were placed in a chilled environment, maintained below martensitic finish temperature, with a suspended weight attached to apply constant stress, as was done in previous studies [29, 31, 30, 33, 32, 34]. An alternating current was applied to heat the specimen into the austenitic phase, and removed to allow the specimen to convectively cool into the martensitic phase.

Four load frames were constructed out of 1" square steel bars to support the specimen and the weight during each test. The specimens were oriented vertically in the current study, rather than horizontally, as had been done with previous studies in order to insure proper alignment of the specimens [31, 32, 34]. A test chamber that enclosed the specimen was constructed using a rapid prototype machine, while allowing for a suspended weight to be attached. An image of a test apparatus, showing the frame and the test chamber, is shown in Fig. 5.

A constant flow of dry filtered compressed air was supplied through a vortex tube, which injected a stream of chilled air into the test chamber to maintain a circulating chilled environment around the specimen. The circulating environment was

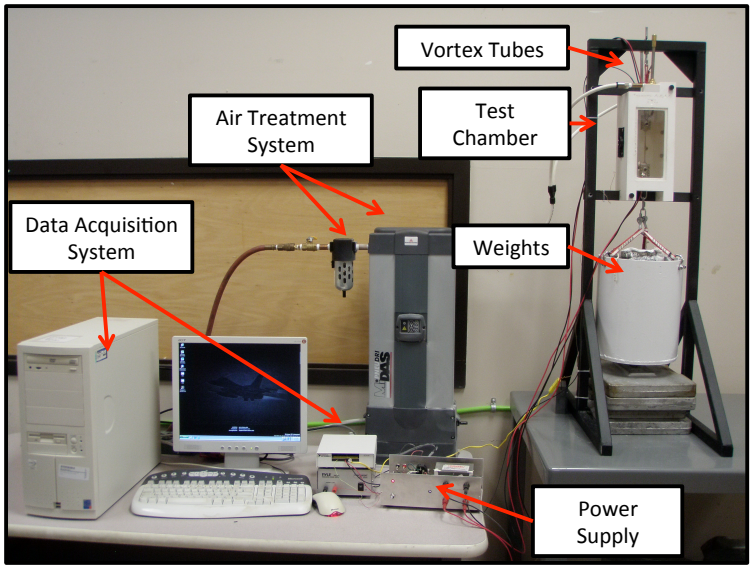

Fig. 5. Testing apparatus used for actuation fatigue testing

maintained between -8 ^{o}C and -15 ^{o}C, which was well below the martensitic finish temperature for the material being tested. An alternating potential, between 1 and 3 V AC at 60 Hz, was placed across specimens and removed to allow specimens to convectively cool. A fixed-ratio transformer was used to drop the voltage from a variable transformer to the desired range, which allowed for a low voltage and high current circuit through the specimen. Voltage was varied by adjusting the variable transformer to achieve optimal heating time without overheating each specimen. Heating took 2-5 sec, depending on the voltage, and cooling phase took 40-60 sec.

Cross sectional area was measured prior to testing at three points along the test gauge (near each end and in the middle) using a micrometer with +/- 0.0254 mm resolution in order to calculate the weight necessary to achieve the desired stress in the specimen. Desired weight was calculated, using the smallest measured cross sectional area along the test gauge, as was done in previous work [34]. A calibrated load cell was used to measure the weight, which was comprised of a weight container,

weight plates and lead beads to accurately achieve the desired weight.

Each specimen was then gripped with pinch grips, which had sharp grooves at the interface with the specimen to create a high friction interaction to prevent any slipping during testing. A custom holder was built using a rapid prototype machine that aligned holes in the gripping section of specimen with holes in the grips to ensure proper alignment and uniform spacing between the grips in all tests. An image of a gripped specimen inside the holder used to attach grips is shown in Fig. 6.

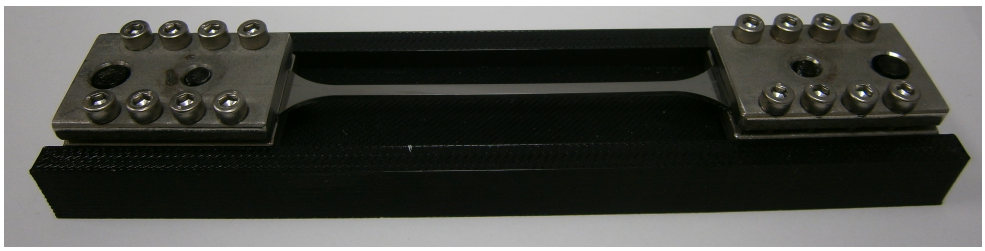

Fig. 6. Image of a gripped specimen in holder used to ensure proper grip alignment

After each specimen was mounted in grips, custom attachment braces were fastened between grips to prevent bending of the specimen during attachment of wire leads and placement in the test chamber. Electrical leads, LVDT extension arm and mounting hardware, which was comprised of shackles, threaded ring and nylon loops, were attached after reinforcement braces were mounted. Electrical leads were attached using a nut and bolt with a locking washer to prevent the leads from loosening during testing through the hole in the gripping section specimen and grips. Specimens were then suspended from a load frame inside the test chamber. An image of a gripped and suspended specimen with electrical leads and support braces attached is shown in Fig. 7.

Once a specimen was mounted in the test chamber, a small weight, 1-3 lb., was suspended from the specimen to maintain tension and alignment. The test chamber

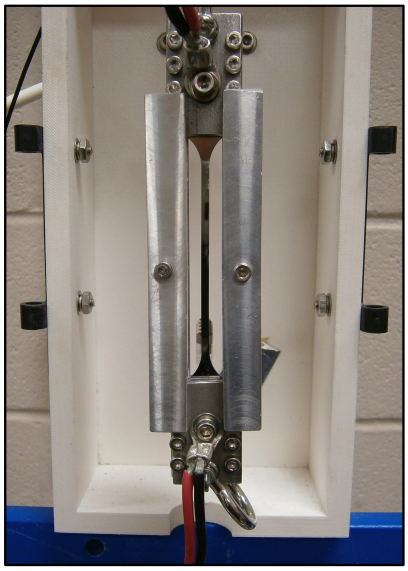

Fig. 7. Image of a suspended specimen with attachment braces fastened to the grips just prior to closing of test chamber and loading

was then closed and the chilled dry air was supplied to the test chamber. The test chamber was allowed to stabilize for at least twenty minutes prior to application of the remainder of the weight..

Displacement of the grip attached to the suspended weight, or bottom grip, was measured using a high precision LVDT mounted outside the test chamber to monitor evolution of strain throughout testing, as shown in Fig. 8. An extension arm that extended outside the chamber to the LVDT was mounted to the the bottom grip, as shown in Fig. 8. Keeping the LVDT outside the test chamber prevented temperature from affecting the measurement. This non-contact method was used, rather than an traditional extensometer, because an extensometer blade would cause a local hotspot during thermal cycling, which in turn would affect the actuation fatigue life of the specimen.

National Instruments LabView was used to control the heating and cooling and record the displacement data during the experiments. A LabView VI program was

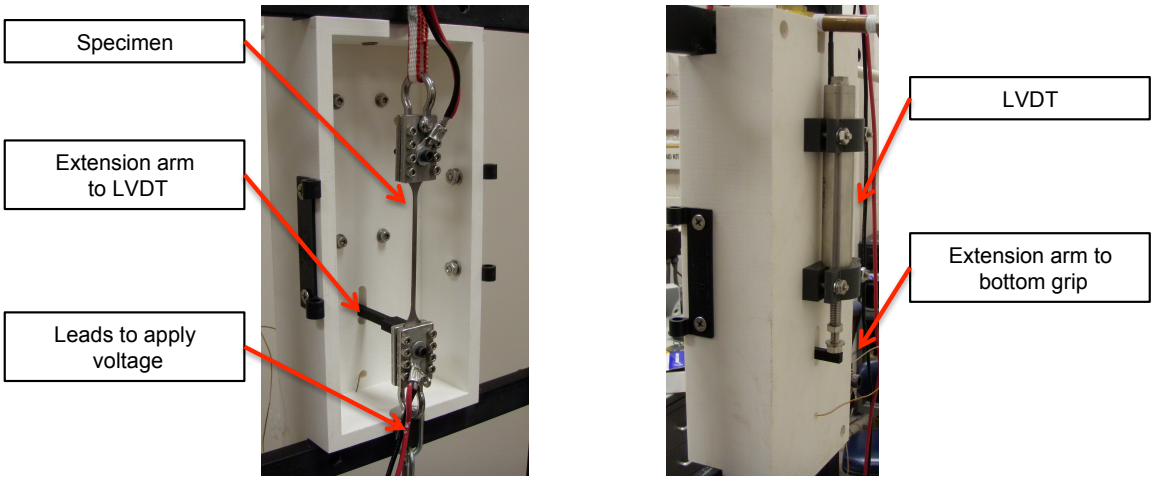

Fig. 8. Test chamber configuration, (a) shows a specimen in the test chamber (b) shows the LVDT mounted to the back of the chamber and (c) shows the extension that connects the bottom grip to the LVDT

written, in which heating and cooling times were inputed for control throughout testing. Heating time was determined for each test by measuring the time it took for material in test gauge to transform from the martensitic phase into the austenitic phase. Applying electrical current resulted in contraction due to temperature-induced transformation and displacement would stabilize, indicating transformation was completed, before significant effects of thermal expansion occurred. Cooling time was set for each test by measuring the time it took for displacement to stabilize in the martensitic phase after heating completed. The LabView program recorded displacement when the specimen was in the austenitic phase, and again in the martensitic phase. Using displacement from the first cycle in the austenitic phase as a reference point, strain was calculated by dividing the change by initial gauge length. The LabView program also recorded temperature inside the test chamber to verify the chamber was maintained below martensite finish temperature.

C. Loading Verification

Infrared imaging and thermocouples where used during preliminary thermal cycling to verify that desired temperatures were achieved and temperature profile was uniform along test gauge during heating and cooling. It was determined that specimens underwent complete transformation with a uniform temperature distribution along, and that strain measurement was accurate when compared to an extensometer.

1. Verfication with Infrared Camera

The first part of verification was to ensure specimens were uniformly heated and cooled, with the entire test gauge cycling through complete transformation. To this end, an infrared (IR) camera was used to observe temperature profile along the test gauge during thermal cycling. Fig. 9 shows images captured using the IR camera, as well as an optical picture of a specimen inside the test chamber for reference. The plexiglass window on the test chamber was replaced with a IR transmitting window in order to accurately capture temperature profile with the IR camera and maintain a closed test chamber environment. The IR camera was calibrated using a thermocouple attached to a specimen and adjusting the emissivity, to account for the IR transmitting window in the IR camera software, until the temperature readings matched between the IR camera and thermocouple.

Temperature appears to be relatively uniform along the test gage in both the austenitic and martensitic phase in Fig. 9. Distribution of temperature along the centerline of a specimen was compared with the austenitic and martensitic finish temperatures to quantify results. Fig. 10 shows temperature distribution along the center of the specimen after heating completed, when the specimen was in the austenitic phase and when the specimen had cooled into the martensitic phase as well as the

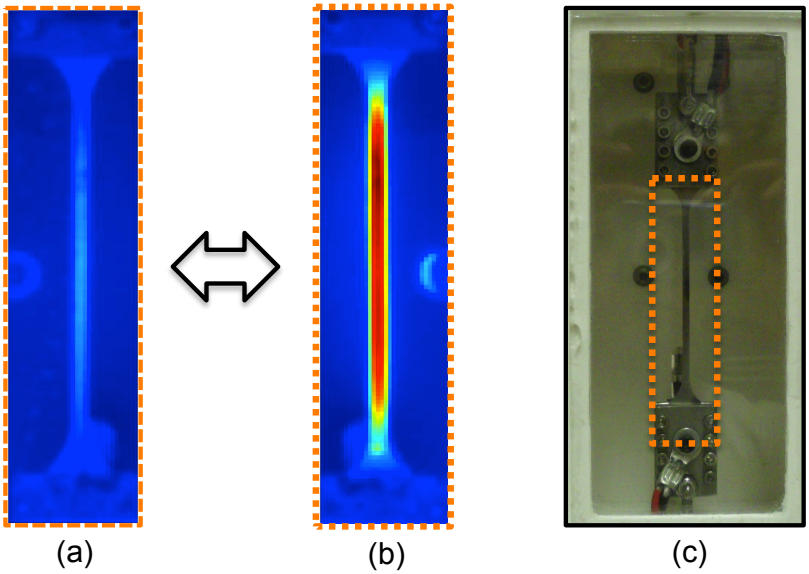

Fig. 9. Test Chamber, (a) IR picture of a specimen just prior application of electrical current, and (b) immediately after current was removed along with (c) and optical image of a specimen in the test chamber

transformation temperatures.

It can be seen that the material in the test gauge was completely below the martensitic finish temperature just prior to the application of the electrical current and above the austenitic finish temperature just after removal of the electrical current, and that the temperature profiles were relatively uniform along the test gauge. From a comparison of temperature profile in every image taken during cycling, it was seen that the highest variation occurred just after removal of the current, which is shown in Fig. 10. The difference between the hottest and coolest point along the test gauge was no more than 20^o C and occurred just after the alternating current was removed.

2. Verification of Strain Measurement

A specimen was thermally cycled on an MTS frame until the thermo-mechanical response stabilized, and strain-temperature response at 200 MPa was observed using

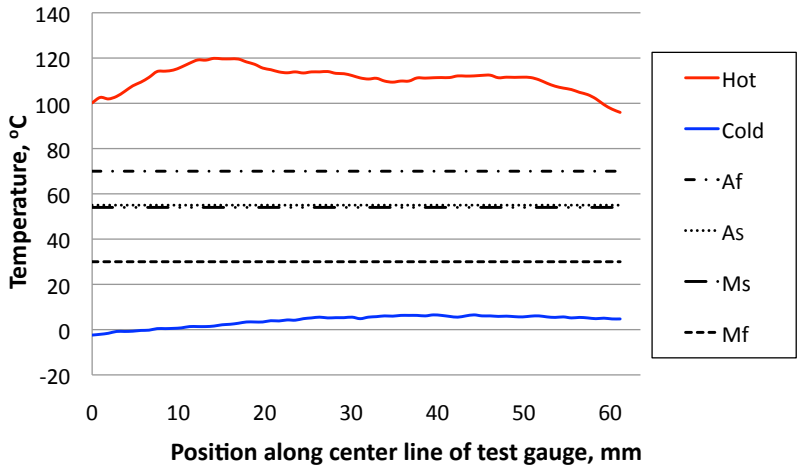

Fig. 10. Plot of the temperature distribution along test gage of a specimen, just prior to and just after application of electrical current compared to critical transformation temperatures at 200 MPa

an environmental chamber and an extensometer for the measurement. The specimen was then placed in the actuation fatigue test apparatus and thermally cycled while under 200 MPa applied stress. Actuation strain was compared between the two different frames, and it was seen actuation strain was measured to be 1.3 % on both experimental setups. It was concluded that measuring strain using an LVDT with the current specimen geometry was comparable to an extensometer by comparing the magnitude of actuation strain.

D. Material Selection and Test Matrix

Actuation fatigue tests were conducted on Ni60Ti40 (wt. %) specimens at 200 MPa to compare the fatigue lives of specimens produced from bulk material from different material suppliers and cutting directions relative to the rolling direction. Ni60Ti40 (wt. %) has been shown to be useful in actuation applications, and was used in the previous work by Schick (2009) [9, 34]. Specimens were produced from bulk material

using EDM, and then heat treated, which consisted of homogenization and aging. Specimens were homogenized at 850^o C for 1 hour in a vacuum and furnaced cooled (heat treatment a) or at 850^o C for 2 hours in an N_2 environment and furnace cooled (heat treatment b). All specimens were aged at 450^o C for 20 hours in an air furnace with a water quench. The resulting transformation temperatures as measured in a previous study with heat treatment a on the same alloy were M_f=20^o C, M_s=24^o C, A_s= 48 ^{o} C, and A_f= 59^o C [34]. The previously measured transformation temperatures are not consistent with all of the specimens in the current study, but provide approximate values that were used for the design of the testing system. Specimen list showing specimen groups and heat treatments are shown in Table I.

Table I. Specimen list for actuation fatigue testing conducted at 200 MPa

Specimen group/ heat treatment	**Number of specimens**	**Material description**
1a	1	$\frac{1}{2}$" plate cut 90^o to rolling direction of plate
2a	3	$\frac{1}{4}$" plate (material used in VGC)
2b	2	$\frac{1}{4}$" plate (material used in VGC)
3a	2	$\frac{1}{2}$" plate cut parallel to rolling direction of plate
3b	2	$\frac{1}{2}$" plate cut parallel to rolling direction of plate
4b	2	$\frac{1}{2}$" plate cut parallel to rolling direction of plate, through the thickness

E. Precipitate Orientation

The microstructure of each specimen was analyzed using an optical microscope after machining, heat treatment, grinding, and polishing. The focus was to ensure polishing resulted in smooth surfaces on the specimens and to observe orientation of the Ni_3Ti precipitates, which were shown to be the location crack initiation in previous studies [32, 34]. Ni_3Ti precipitates were observed to be ellipsoidal, with varying sizes, aspect ratios that ranged from 1 to greater than 10, and orientations within specimens from micrographs. Microstructure of each specimen was characterized into one of three categories by orientation of the long axis of ellipsoidal Ni_3Ti precipitates: parallel, parallel with variation and perpendicular with variation relative the loading direction. Micrographs taken of surfaces from each group and heat treatment are shown in Figs. 11-15.

A micrograph captured prior to testing of a surface of the specimen in group 1a is shown in Fig. 11. It is seen that Ni_3Ti precipitates were mostly oriented within

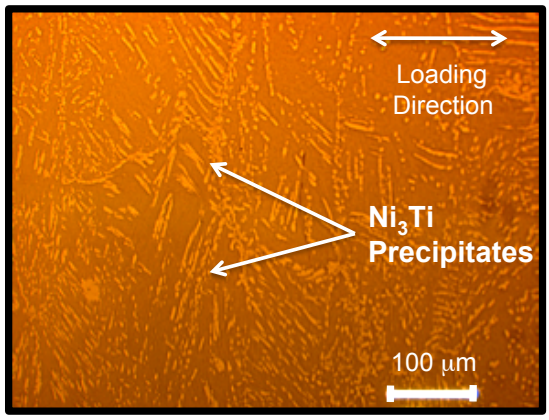

Fig. 11. Micrograph from a specimen in group 1a showing precipitate orientation perpendicular with variation to the loading direction

45^o of perperdicular to the loading direction, so this specimen was grouped into the category of perpendicular with variation. The ellipsoidal precipitates on the surface

of the specimen had a major axis as long as 100 μm.

Specimens in group 2a had a similar orientation to that observed in group 1a, but Ni_3Ti precipitates were smaller. Fig. 12 shows a micrograph of the surface of a specimen from group 2a prior to testing. In the image, is it observed that precipitates

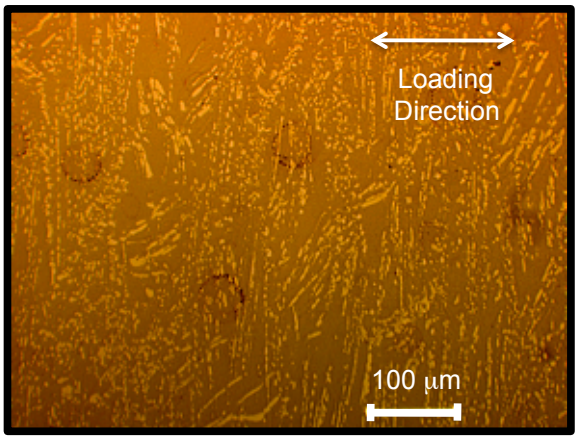

Fig. 12. Micrograph from a specimen in group 2a showing precipitate orientation perpendicular with variation to the loading direction

were oriented more than 45^o from the loading direction. The maximum length of the major axis of the ellipsoidal precipitates was observed to be less than 70 μm.

The specimens from the same group but with the additional hour of homogenization, had precipitates oriented differently relative to the loading direction of the specimen. An image taken of the surface of a specimen from group 2b is shown in Fig. 13. From the image, it is observed that precipitates were nearly completely oriented within 45^o of loading, and mostly within 30^o of the loading direction. The length of the major axis of the ellipsoidal precipitates was as large as 100 μm.

Specimens in group 3a had a precipitates oriented similarly to specimens in group 2b. An image of the surface of an untested specimen is shown in Fig. 14. The precipitates were mostly aligned within 45^o of the loading direction. Precipitates were observed to be as long as 100 μm. It was not possible to take an image of the surface

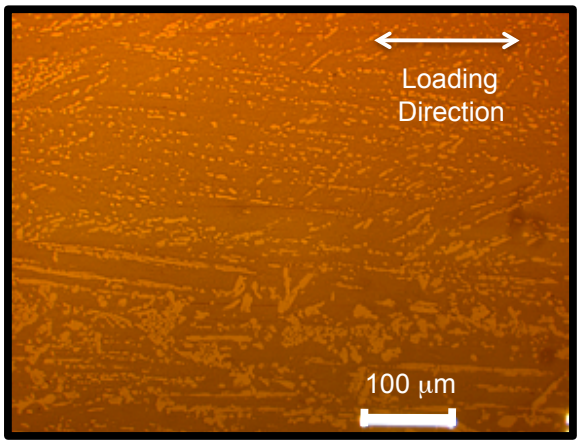

Fig. 13. Micrograph of a specimen from group 2b showing precipitate orientation parallel with variation to the loading direction

of a specimen from group 3b, due to a broken lens. However, the microscope was still functional, so microstructure was analyzed without a digital image. Analysis showed that precipitates were oriented within 45^o of loading, and were as large as 100 μm.

The specimens with the most uniform precipitate orientation were in group 4b. An image of the microstructure is shown in Fig. 15. From the image, it is seen that precipitates were all uniformly aligned with loading. Precipitates were all smaller than 70 μm along the major axis, and had a range of aspect ratios from nearly circular to almost cylindrical. Precipitate orientation of this group was very similar to that observed in specimens tested by Schick (2009) [34].

A few observations can be made from a comparison of all of the microstructures from all of the specimen groups. The maximum length of the major axis on the ellipsoidal precipitates ranged from 70 to 100 μm. Most Ni_3Ti precipitates were observed to be ellipsoidal in shape with high aspect ratios. Orientation of these precipitates varied amongst specimens but was consistent within each specimen group, and no clear determination can be made if orientation depended on the initial cold rolling or if the orientation changed with the homogenization time. Specimens in group 2

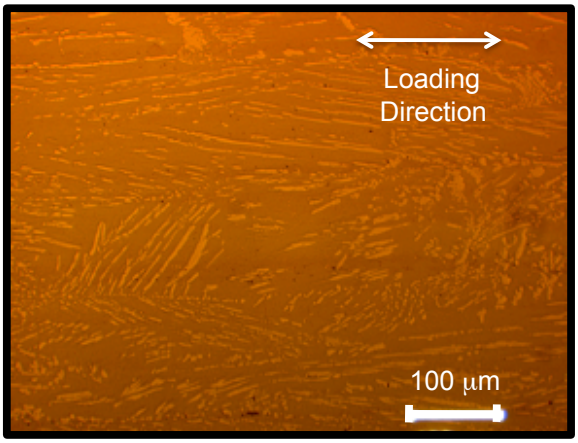

Fig. 14. Micrograph from a specimen in group 3a showing precipitate orientation parallel with variation to the loading direction

had different orientations between the two different homogenization heat treatments, but specimens in group 3 had the same orientation between the homogenization heat treatments.

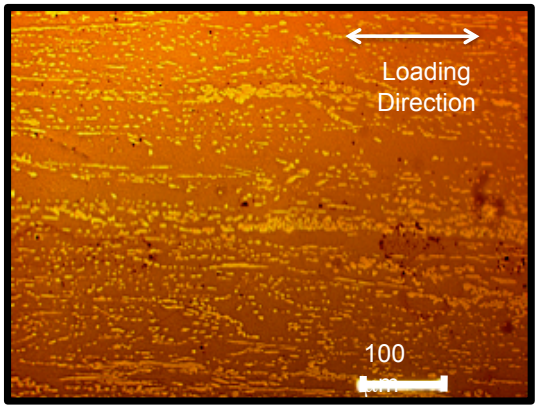

Fig. 15. Micrograph from a specimen in group 4b showing precipitate orientation uniformly parallel to the loading direction

CHAPTER III

TESTING RESULTS

After testing completed, the results and specimens were analyzed. Evolution of strain through thermal cycling was analyzed and was found to depend on the homogenization time and precipitate orientation. Actuation fatigue lives were compared amongst the specimen groups previously described and found to increase with homogenization time, and depend on precipitate orientation. Postmortem analysis of specimen surfaces showed cracking behavior in and around the Ni_3Ti precipitates varied with orientation relative to loading.

A. Strain Evolution

The position of the bottom grip was recorded when the material in the test gauge was in the austenitic and martensitic phase during each cycle, as previously described in Chapter III. Strain when the specimen was in the austenitic and martensitic phase was calculated for each cycle, as well as the actuation strain, which was defined as the difference between the strain in austenite and martensite for each cycle. Plots of the evolution of the three strains through the life of a specimen from each group are shown in Figs. 16-20. The first result presented in Fig. 16 the evolution of a specimen from group 2a, which had been homogenized for 1 hour. The specimen shown failed after 5,592 cycles. The actuation strain was 1.1%, and had a total of 1.6% irrecoverable strain at failure.

The next result shown is from a specimen from the same group, but underwent an 2 hours of homogenization in a nitrogen environment rather than 1 hour in a vacuum. Fig 17 shows the strain evolution from a specimen in group 2b. The specimen shown from group 2b failed after 10,375 cycles. The actuation strain was constant

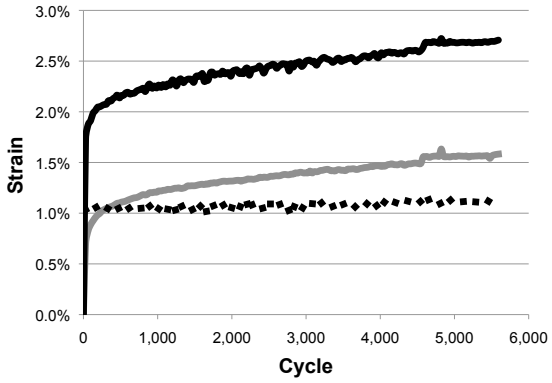

Fig. 16. Strain evolution showing the strain in martensite (black), strain in austenite (gray), and actuation strain (dashed) for representative specimens for a specimen from group 2a

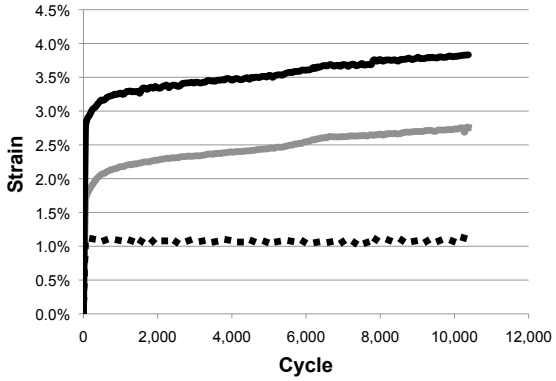

Fig. 17. Strain evolution showing the strain in martensite (black), strain in austenite (gray), and actuation strain (dashed) for representative specimens for a specimen from group 2b

throughout the life at 1.1%, and had a total of 2.8% irrecoverable strain at failure.

Results from a specimen in group 3 that underwent homogenization in a vacuum for one hour (group a) is shown in Fig. 18. The specimen shown from group 3a

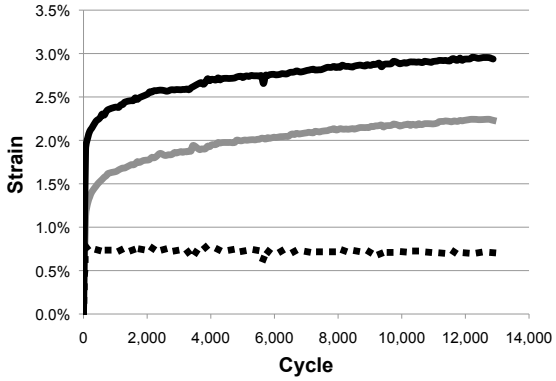

Fig. 18. Strain evolution showing the strain in martensite (black), strain in austenite (gray), and actuation strain (dashed) for representative specimens for a specimen from group 3a

failed after 12,871 cycles. The actuation strain was constant throughout testing at 0.7%, and had a total of 2.2% irrecoverable strain at failure. The irrecoverable strain accumulated quickly in the initial cycles then stabilized and then grew slowly.

The next result shown is from a specimen in group 3 that underwent two hours of homogenization in a nitrogen atmosphere. Fig. 19 shows an evolution of the strain of a specimen from group 3b. The specimen shown from group 3b failed after 45,038 cycles. The actuation strain was had an actuation strain was 0.9%, and had a total of 3.7% irrecoverable strain at failure. In this experiment, the irrecoverable strain accumulated quickly and eventually stabilized without accumulating any additional irrecoverable strain after approximately 25% of the life.

The final strain evolution result presented is from a specimen in group 4 that underwent two hours of homogenization in a nitrogen atmosphere. The specimen shown from group 4b failed after 21,264 actuation cycles. The actuation strain was

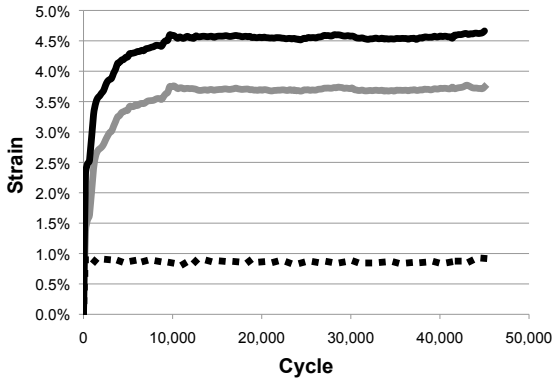

Fig. 19. Strain evolution showing the strain in martensite (black), strain in austenite (gray), and actuation strain (dashed) for representative specimens for a specimen from group 3b

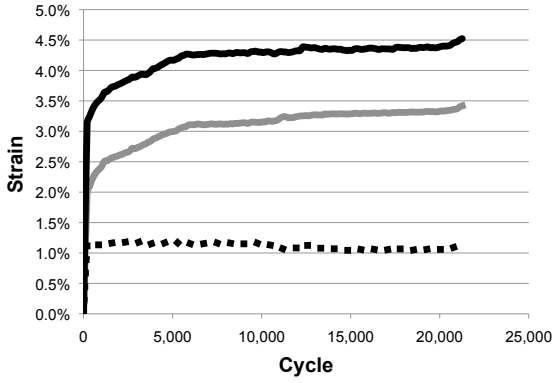

Fig. 20. Strain evolution showing the strain in martensite (black), strain in austenite (gray), and actuation strain (dashed) for representative specimens for a specimen from group 4b

1.1% throughout the life of the specimen and had 3.4% irrecoverable strain at failure.

From Figs. 16-20 a general trend of specimens with increased irrecoverable strain resulted in increased actuation fatigue life. The irrecoverable strain evolution is plotted on one graph and shown in Fig. 21 to illustrate this trend. The plot shows that

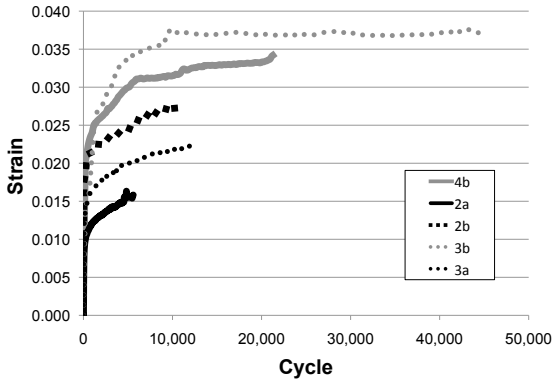

Fig. 21. Irrecoverable strain evolution for specimens from each of the specimen groups.

the specimens that stabilized at the highest level of irrecoverable strain underwent the greatest number of cycles to failure. Irrecoverable strain is the result of retained martensite, damage and transformation-induced plasticity in general. This stabilization was relatively early in the life of the specimens, usually within 5-10% of the total number of transformation cycles, so damage accumulation does not account for a significant part of the irrecoverable strain. Generation of retained martensite does not cause irrecoverable strain, as this would likely cause a change in the actuation strain through cycling, and the actuation strain was observed to remain constant through actuation cycling. As such, stabilized irrecoverable strain is predominantly comprised of transformation induced plasticity. Plasticity served as a mechanism to reduce the local stress concentrations by generating a residual stress field, and local stress concentrations decreased as irrecoverable strain increased. The reduction in localized stress concentrations and the stress amplitudes through repeated transfor-

mation resulted in longer fatigue lives, as cracks are less likely to occur when the stress is reduced. It is also seen that specimens with increased homogenization time accumulated more irrecoverable strain through cycling, which in turn increased actuation fatigue life through the same mechanism.

B. Actuation Fatigue Life Results

The number of cycles to failure for each of the specimen groups described in Chapter III were averaged and are presented in Table II. Strain evolution data was lost due to

Table II. Comparison of actuation fatigue life for each specimen group tested at 200 MPa

Specimen group	**Number of specimens**	**Average number of cycles to failure**	**Actuation strain**
1a	1	4,959	-
2a	3	6,100	1.1%
2b	2	9,200	1.25%
3a	2	13,700	0.8%
3b	2	40,600	0.9%
4b	2	27,200	1.1%

grounding issues with the LVDT and also a current spike in the LVDT that resulted in corrupted readings, as was the case in the specimen from group 1a, one of the specimens in group 2a, 3a, 3b, and 4b. The inaccurate readings from the LVDT reading affected the strain data, but did not affect the actuation fatigue life of the specimens. Response of the specimens was monitored at least twice a day to ensure the specimens were undergoing complete transformation without any over heating for

all of the tests performed. It is concluded that material processing has a significant result on the actuation fatigue life and actuation strain behavior based off the results in Table II. It is seen that specimens that underwent 2 hours of homogenization underwent more transformation cycles before failure than specimens homogenized in a vacuum for only one hour from a comparison of the results in groups 2 and 3. The additional hour of homogenization increased fatigue life of the specimens by roughly 30%, and also increased actuation strain in specimen group 2. Similarly, the additional hour of homogenization increased fatigue life of the specimens in group 3, but in this case by a factor of almost 3, and increased actuation strain by 12.5%. Increased actuation strain combined with the longer fatigue life, makes two hour homogenization more desirable for fatigue life performance as more work is being done per cycle. The additional hour of the homogenization at 850^o C causes a change in response of the material in both the transformation behavior and its ability to resist crack initiation and growth, rather than the environment, as the difference in the environment would affect mainly the surface of the specimens, which was removed during polishing and grinding.

1. Effects of Precipitate Orientation

A comparison of the different precipitate orientation groups was conducted to observe a change. Table III shows average fatigue life at 200 MPa of the three different precipitate orientation groups previously described catagorized by homogenization time.

It can be seen that the precipitate orientation relative to the loading direction has a drastic effect on fatigue life. It is seen that specimens with precipitates oriented parallel with variation to the loading direction had longer fatigue lives than specimens with precipitates oriented perpendicular to the loading direction by comparing the

Table III. Comparison of average actuation fatigue life for various specimen sets with the precipitate orientation with respect to the loading direction

Precipitate orientation with respect to loading direction	**Heat treatment**	**Number of specimens**	**Number of cycles to failure (Avg.)**
Perpendicular with angulation	a	4	6,100
Parallel with angulation	a	2	13,700
Parallel with angulation	b	4	25,900
Parallel	b	2	27,200

results of specimens that underwent 1 hour of homogenization. It is seen that variation in the precipitate orientations does not have a drastic effect by comparing results of the specimens that underwent 2 hours of homogenization.

C. Postmortem Micrographs

After testing was completed, micrographs were taken of specimen surfaces to observe cracking. The first micrograph presented shows the postmortem surface of a specimen with precipitates uniformly oriented parallel to the loading. An image taken near the fracture surface of a specimen in group 4b is shown in Fig. 22.

Approximately 50 auxiliary cracks that did not cause ultimate failure are observed, all of which are in contact with at least one Ni_3Ti precipitate in the image. Most cracks are through Ni_3Ti precipitates, with little evidence of cracking starting at the interface between precipitates and matrix material.

Specimens with precipitates oriented parallel to the loading direction with variation showed a different cracking behavior. A micrograph taken near fracture surface

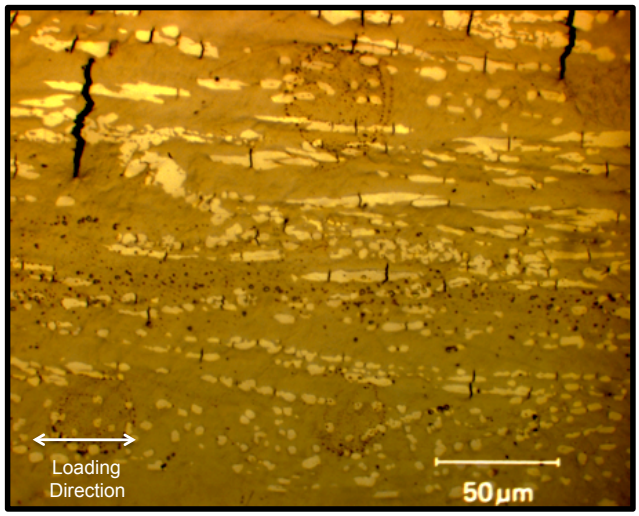

Fig. 22. Micrograph of postmortem surface of a specimen precipitates oriented parallel to the loading direction

on a specimen from group 3a, which had precipitates oriented parallel with variation to the loading, is shown in Fig. 23. It was seen that all cracks are in contact with at least on Ni_3Ti precipitate. Though, less cracking was observed in this specimen in this specimen, than specimens with uniformly oriented precipitates. In this image, there is a combination of precipitates cracking and interface cracking between precipitates and matrix material. Cracks in this image are smaller and more sparse than in the uniformly parallel orientation.

Specimens with precipitates oriented perpendicular to loading direction with variation were analyzed after testing, which showed the cracking behavior to be different from the two previous specimens shown. Cracking was less predominant, so finding cracks was more difficult. As such, the entire specimen had to be analyzed rather than just in the proximity to the fracture surface. A micrograph taken away from the fracture surface of a specimen from group 2a is shown in Fig. 24. Only one auxiliary crack is observed, which 30 μm long and in contact with multiple Ni_3Ti precipitate. The observed crack did not initiate in a precipitate but rather at interface between

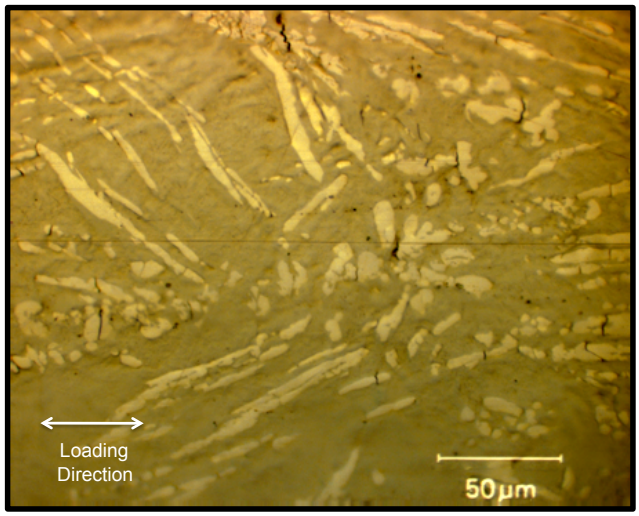

Fig. 23. Micrograph of postmortem surface of a specimen precipitates oriented parallel with variation to the loading direction

the precipitate and the matrix material.

1. Discussion

A key consideration in material selection of SMAs to be used in actuators is considering both the structural and functional fatigue response of these metals. The generation of large irrecoverable strain in an actuator could lead to failure of the actuator to perform its intended function, but if the material can not undergo sufficient temperature-induced transformation cycles the actuator would fail due to rupture. Increasing the homogenization time of the SMA increases the number of cycles before rupture, as the specimens with the the increased homogenization time, had much longer actuation fatigue lives. However, increased homogenization time had the disadvantage of greater irrecoverable strain at failure. As there is a trade-off between the generation of irrecoverable strain and actuation fatigue life, there is not an ideal heat treatment for all applications. It would be beneficial to use a short homogenization heat treatment time for applications that require tight tolerances and few

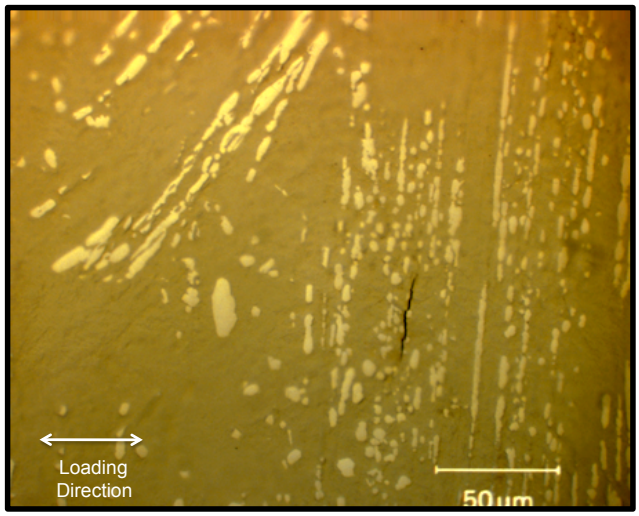

Fig. 24. Micrograph of postmortem surface of a specimen precipitates oriented parallel with variation to the loading direction

actuation cycles. However, increasing homogenization time would be beneficial if a design requires a large number of cycles prior to failure, but it would require that the material is thermally cycled to stabilize the accumulation of irrecoverable strain prior to use.

Another key consideration for the use of Ni-rich SMAs in actuators is the orientation of the Ni-rich precipitates. It was seen that cracking behavior was drastically affected by precipitate orientation. The highest crack density at failure was observed in specimens with precipitates uniformly oriented to the loading direction, which also had the longest fatigue life of specimens tested. Cracks initiated inside precipitates oriented with the loading direction, which is likely caused by a drastic increase in stress inside the precipitate as matrix material transforms from the austenitic to martensitic phase. The interaction of precipitates and matrix material cause cracking, and when oriented parallel to the loading direction reduce crack growth rates. Crack growth rates have been observed to be high under pseudoelastic loading for nearly equi-atomic NiTi material, similar to the matrix material in the current specimens [26]. Reduced

crack growth rates, allow for many cracks to initiate before ultimate failure. Little to no auxiliary cracks and the shortest fatigue lives were observed in specimens with precipitates oriented perpendicular with variation to the loading direct. Cracks initiated at the interface between precipitates and matrix material, indicating there was not as large of a stress rise in precipitates oriented perpendicular to loading through transformation. Precipitates caused crack initiation, but did not affect crack growth rates due to their orientation. As such, a crack would initiate, grow quickly and cause ultimate failure before other cracks could initiate. It is concluded that favorable precipitate orientations can increase fatigue life, by decreasing actuation fatigue crack growth rates, though it changes the cause for crack initiation and increases crack density at failure.

CHAPTER IV

NUMERICAL INVESTIGATION

A numerical investigation was conducted to illustrate stress distribution in and around an elastic precipitate inside a transforming matrix in an effort to further explain the change in cracking behavior described in Chapter III. A 2-D plane stress unit cell comprised with four uniformly distributed precipitates inside a transforming matrix was modeled under actuation loading. Plane stress conditions were used to simulate surface conditions where cracking was observed. Results were used to explain the change in cracking behavior observed during actuation fatigue testing.

A. Unit Cell Development

A boundary value problem was defined to show the response of an elastic precipitate inside of a transforming SMA matrix. A square unit cell with four uniformly distributed precipitates was used to capture observed precipitate orientations. A schematic of the unit cell is shown in Fig. 25.

It can be seen that the system can be reduced to quarter symmetry from the schematic shown, which allowed for the reduced boundary value problem depicted in Fig. 26. Periodicity and symmetry of the initial unit cell required horizontal boundaries remained horizontal and vertical boundaries vertical due to symmetry in the reduced unit cell. Deflection in the x-direction on the left boundary of the body was fixed at zero, and the right boundary was allowed to move in the x-direction, but deflection was uniform along the boundary. Similarly, the bottom boundary was fixed in the y-direction and the top boundary was allowed to uniformly move in the y-direction. Loading was done in multiple steps. The body started unloaded at 227 ^{o}C (A_f+120 ^{o}C), which was well above the austenitic finish temperature, and the

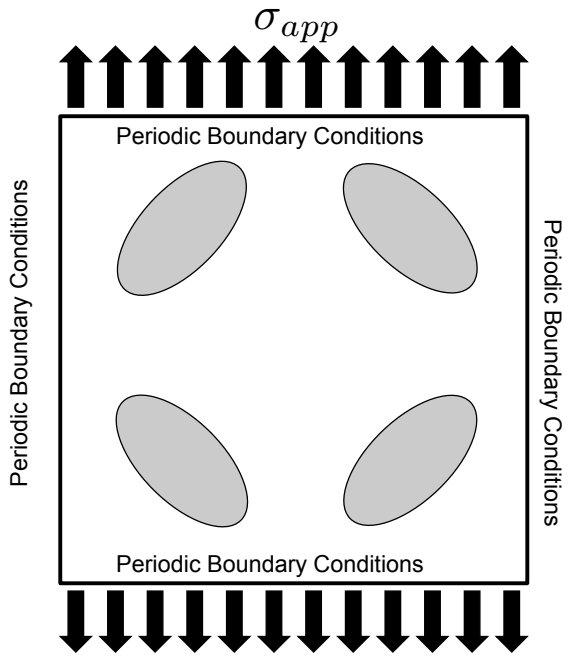

Fig. 25. A schematic of the plane stress unit cell of the precipitate matrix system

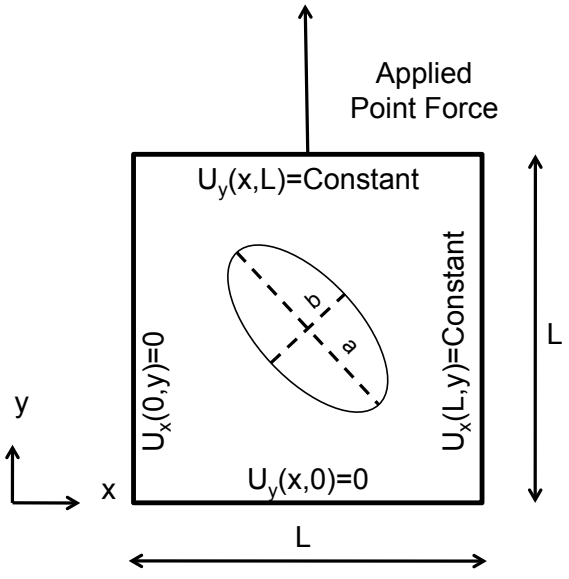

Fig. 26. Schematic modeled plane stress boundary value problem

point load was incrementally applied to achieve an average stress of 200 MPa in the y-direction, to reflect the loading seen in the actuation fatigue experiments. The applied load remained constant while the temperature was lowered to 27 ^{o}C (M_s-24 ^{o}C), which ensured the matrix was completely in the martensitic phase.

The precipitate was modeled as a linearly elastic material, and the SMA matrix was modeled using a non-linear constitutive model. The constitutive model used to describe the thermo-mechanical response of SMA matrix was the numerical implementation of the Boyd-Lagoudas (1996) model, details of which can be found in Quidwai and Lagoudas (2000) and Hartl et. al (2011) [37, 38, 39]. Simulations were conducted using ABAQUS finite element software with approximately 3,300 2-D plane stress quadratic elements with reduced integration, type **CPS8R** [40]. The mesh was set to have at least 50 elements along each boundary. An example of a mesh used for this simulation is shown in Fig. 27.

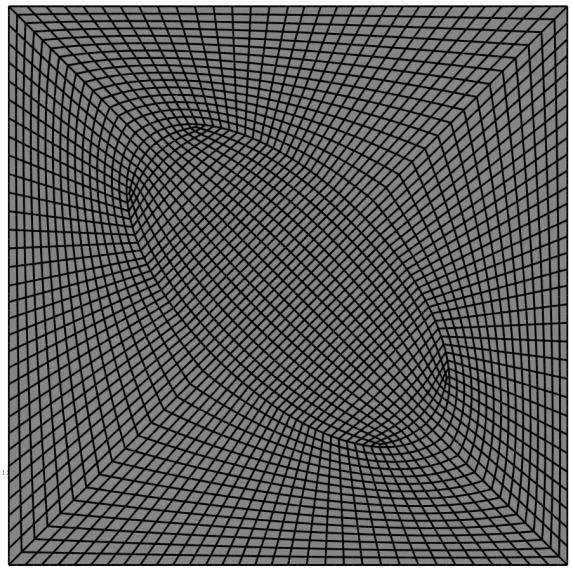

Fig. 27. An example of the mesh with 3,273 elements used to simulate a precipitate with an aspect ratio of 2 oriented 45^{o} from the loading direction

1. Defining Model Parameters

The area fraction of the precipitate remained constant throughout all of the 2-D simulations. As such, the aspect ratio, orientation and volume fraction uniquely defined the geometry for each simulation. The aspect ratio of the precipitate for this study is defined as the major axis length, a, of the precipitate divided by the minor axis length, b. Orientation of precipitates was defined at the angle between the long axis and loading direction. Four different aspect rations were used, which were 1, 1.5, 2 and 2.5, with three different orientations, 0^o, 45^o and 90^o for the simulations. Images of microstructure taken using a scanning electron microscope (SEM) were used to define area fraction of Ni_3Ti precipitate in the unit cell. Images were converted to binary images, in which Ni_3Ti precipitates were converted to white and transforming matrix and other Ni-rich precipitates were converted to black. An SEM image of the microstructure along with the corresponding binary image is shown in Fig. 28.

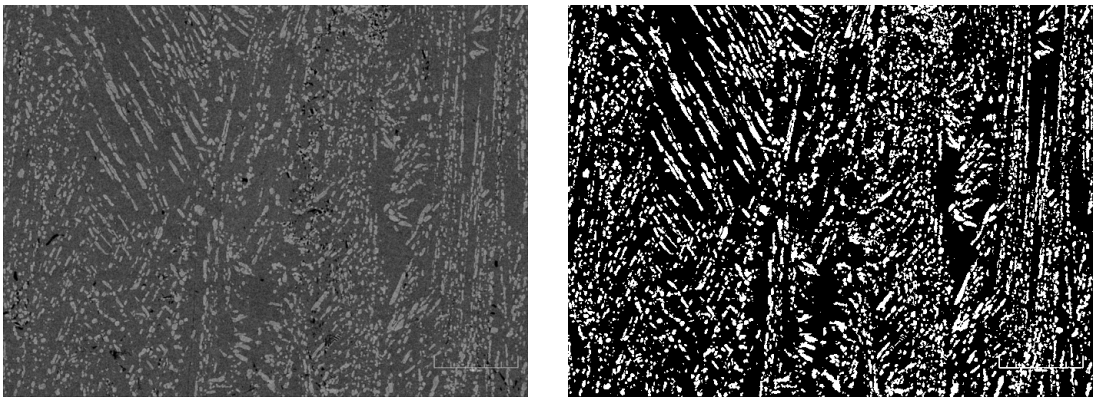

Fig. 28. Image of microstructure of Ni60Ti40 (wt. %) taken using an Scanning Electron Microscope (A) and the corresponding binary conversion (B)

Numerically a greyscale image is simply an 2-D array with each value corresponding to a pixel and ranged from 0 to 256. Greyscale pixel values are set to 1 if they are

in the predetermined range consistent with the Ni_3Ti precipitates and 0 elsewhere to convert an image to a binary. Area fraction is calculated by summing values for each pixel and dividing by the total number of pixels. Area fraction was calculated to be 21.5% from the image shown in Fig. 28. Dimensions of simulated precipitates were calculated using the formulas given in eqs. 4.1-4.2 using area fraction.

$$a = L\sqrt{\frac{R\ A_f}{\pi}} \tag{4.1}$$

$$b = \frac{a}{R} \tag{4.2}$$

In these equations, a and b are dimensions of the precipitate shown in Fig. 26, R is apect ratio, A_f is area fraction of the precipitate, and L is length of the reduced unit cell.

Elastic modulus of the precipitate was taken from results of nano-indentation experiments presented in Bertachinni (2009) [32]. The measured modulus of the precipitates decreased as depth of the the nano-indenter increased. The highest measured value was used for current simulations.

Maximum transformation strain was determined iteratively in order to have the effective actuation strain with a circular precipitate was approximately 1.1%, which was consistent with the results of tests conducted on specimens in groups 2a and 4b presented in Chapter III. Remaining SMA parameters were taken from typical equiatomic values, aside from thermal expansion, which was neglected for the current study. A complete list of parameters used are shown in Table IV.

Table IV. Model parameters used for FEA simulations

Parameter	**Value**	**Description**
E_p	165 GPa	Elastic modulus of the precipitate
ν_p	0.3	Poisson's ratio of the precipitate
E_a	69.3 GPa	Elastic modulus of the Austenitic phase
E_m	37.6 GPa	Elastic modulus of the Martensitic phase
ν_a	0.33	Poisson's ratio of the Austenitic phase
ν_m	0.33	Poisson's ratio of the Martensitic phase
M_s	61 ^{o}C	Martensitic start temperature
M_f	51 ^{o}C	Martensitic finish temperature
A_s	100 ^{o}C	Austenitic start temperature
A_f	107^{o}C	Austenitic finish temperature
C_M	8.7 MPa/^{o}C	Stress influence coefficient of Martensite
C_A	7 MPa/^{o}C	Stress influence coefficient of Austenite
σ_{cal}	7 MPa/K	Calibration stress
H_{min}	0	Minimum transformation strain
H_{max}	0.06	Maximum transformation strain
σ_{tc}	0.02 MPa	Stress at transformation is non-zero
k_t	0	Exponent used for maximum transformation strain
η_1	0.2	Smooth hardening parameter
η_2	0.2	Smooth hardening parameter
η_3	0.2	Smooth hardening parameter
η_4	0.2	Smooth hardening parameter

B. Results

It was seen that stress varied inside precipitates when the matrix was in the austenite and martensite phases. Images of stress distribution when the matrix material is in the austenitic and martensitic phases are shown in Figs.29-32 to show the change in stress distribution. Fig. 29 shows the resulting Von Mises stress distributions from a simulation conducted with an aspect ratio of 1. Von Mises stress is highest inside the

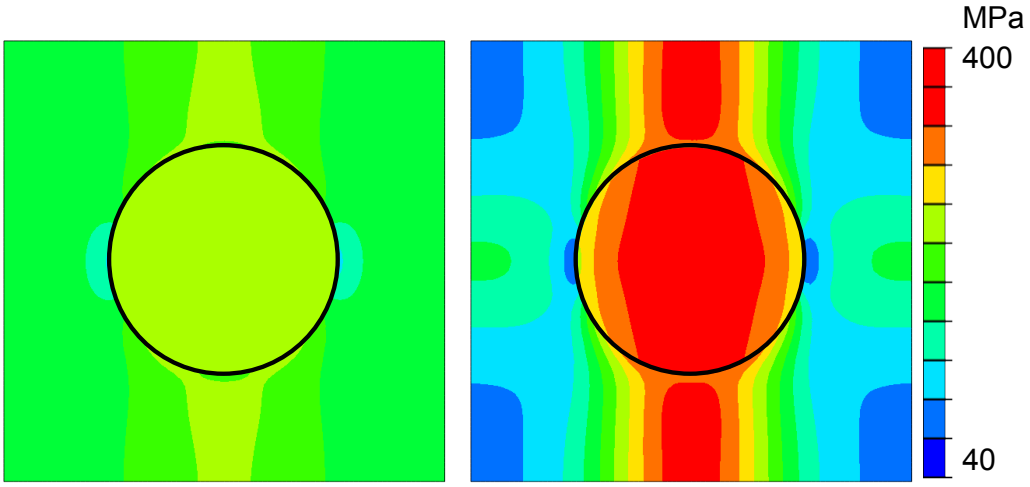

Fig. 29. Von Mises stress field for precipitate with aspect ratio of 1 with matrix in the austenitic phase (left) and with the matrix in the martensitic phase (right)

precipitate and just above or below the precipitate in the matrix, not at the interface between the matrix and the precipitate. It is also observed that stress rises due to transformation are much greater than rises due to elastic stiffness differences between precipitate and matrix, as stress in the precipitate is much greater when the matrix is in the martensitic phase.

Figs. 30-32 show distribution of Von Mises stress in the reduced unit cell with an aspect ratio of 1.5 to illustrate the effect of precipitate orientation. Fig. 30 shows an image of Von Mises stress distributions when the matrix was in the austenitic

and martensitic phases for the precipitate oriented with direction of loading. Von

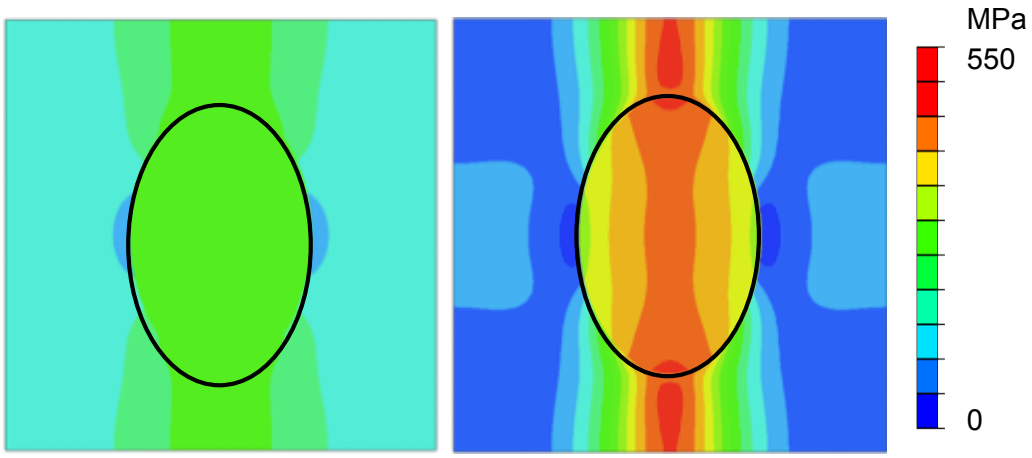

Fig. 30. Von Mises stress field for precipitate with aspect ratio of 1.5 oriented parallel to the direction of loading with matrix in the austenitic phase (left) and with the matrix in the martensitic phase (right)

Mises stress fields from results of a simulation of a precipitate with an aspect ration of 1.5 oriented 45^o to loading direction is shown in Fig.31. Von Mises stress fields from results of a simulation of a precipitate with an aspect ration of 1.5 oriented perpendicular to loading is shown in Fig.32.

It is seen that stress inside precipitates decreases as the angle between the major axis of the precipitate increases in Figs. 30-32. It is also observed that stress in the regions directly adjacent in the x-direction to precipitates oriented parallel to the loading direction is low compared to the rest of the matrix. Decreased stress in these regions is cause for slow crack growth observed in specimens with uniformly oriented precipitates, as described in Chapter III.

High stress regions seen in matrix material are lowered after repeated transformation due to transformation induced plasticity. Transformation induced plasticity would relax the stress in the high stress regions in the material due to generation of a residual stress field, and would in turn, lower cyclic stresses in these regions.

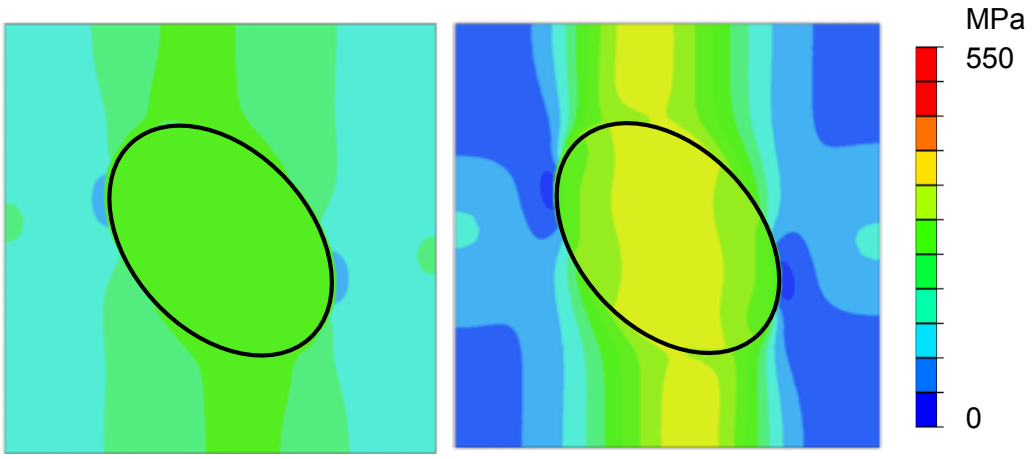

Fig. 31. Von Mises stress field for precipitate with aspect ratio of 1.5 oriented 45^o to the direction of loading with matrix in the austenitic phase (left) and with the matrix in the martensitic phase (right)

Lower cyclic stresses would increase number of cycles prior to crack initiation and slow growth after crack initiation.

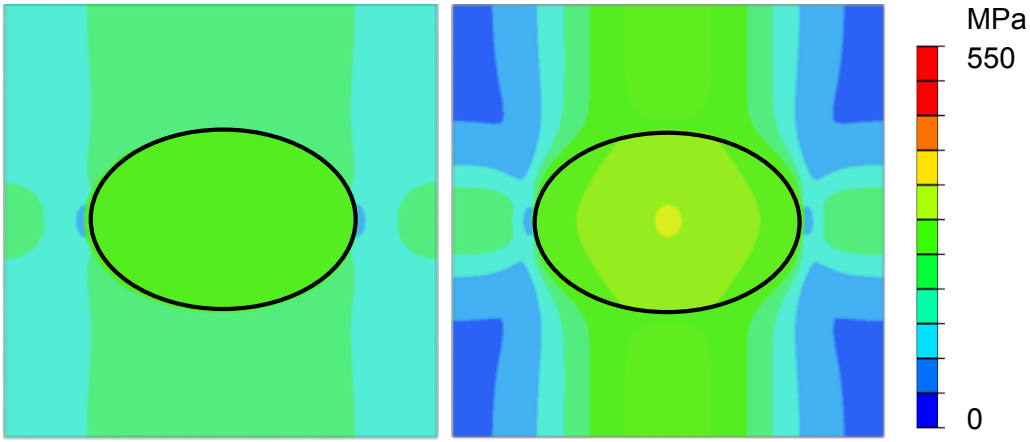

Fig. 32. Von Mises stress field for precipitate with aspect ratio of 1.5 oriented perpendicular to the direction of loading with matrix in the austenitic phase (left) and with the matrix in the martensitic phase (right)

1. Stress in the Precipitates

Simulations were run with plane stress conditions to reflect the loading on the precipitates on the surface of the specimens were cracking was observed to initiate. Von Mises stress at the center of the precipitate when the matrix was in the austenitic phase, after loading, and when the matrix was in the martensitic phase, was compared amongst all of the simulations. A complete comparison of Von Mises stress at the center of the precipitate is shown in Table V.

Table V. Von Mises stress at center of precipitate

Aspect ratio	**Orientation angle**	**Stress in austenite (MPa)**	**Stress in martensite (MPa)**
1	-	249	400
1.5	0	268	468
	45	250	390
	90	238	368
2	0	284	520
	45	246	367
	90	233	362
2.5	0	300	574
	45	244	354
	90	232	370

It is seen that Von Mises stress inside precipitates when the matrix is in both phases is higher when precipitates are oriented parallel to loading direction. Significantly lower stresses inside precipitates oriented perpendicular to loading is likely

why cracking was not observed inside precipitates with this orientation in postmortem analysis of fatigue specimens. It is also observed that stress inside precipitates increases with aspect ratio.

Another key consideration in cracking behavior of the precipitates would be the cyclic stress amplitudes that would be experienced inside precipitates, as cracking may not be caused by one transformation cycle but by repeated transformation. Predicted Von Mises stress inside the precipitates was never greater than 600 MPa, which could potentially be below the ultimate strength of the Ni_3Ti precipitates. The cyclic stress amplitude inside the precipitate is greatest with the highest aspect ratio oriented parallel to the loading and least with the highest aspect ratio oriented 45^o from the loading direction. The large difference in stress indicates cracking is more likely to occur in precipitates with large aspect ratios oriented parallel to the loading. From postmortem analysis shown in Chapter III it was seen that cracking inside precipitates occurred most predominantly in precipitates with high aspect ratios.

2. Effective Actuation Strain Comparison

Actuation strain was compared amongst different orientations and aspect ratios for all simulations conducted. Effective actuation strain was calculated by dividing deflection at the point of load, or top of the unit cell, by the characteristic length, L. Table VI shows the calculated effective actuation strain values for all simulations.

It is seen that precipitates oriented parallel to the loading direction resulted in lower actuation strain as the aspect ratio increased. Results in the simulation indicate a large reduction in actuation strain, by comparing the results of specimens from group 4b and 2b, which were cut with the same orientation relative to the rolling direction and underwent the same heat treatment, this trend was observed and described in Chapter III. Specimens from these 2 groups had an actuation strain

Table VI. Effective actuation strain for all of the simulations conducted

Aspect ratio	**Orientation angle**	**Measured actuation strain**
1	-	1.08%
1.5	0	1.00%
	45	1.05%
	90	1.11%
2	0	0.90%
	45	1.09%
	90	1.13%
2.5	0	0.80%
	45	1.10%
	90	1.11%

that varied by 13.6%. Actuation strain in FEA results varied by 30% between the unit cell with precipitates of aspect ratio of 2.5 oriented parallel to loading, and when precipitates were oriented 45^o to the loading. While this may not completely account for the complete difference in measured actuation strain amplitude between the specimens, it does show precipitate orientation may break isotropy of the material.

CHAPTER V

WORK-BASED METHOD TO ACTUATION LIFE PREDICTION

Along with identification of failure mechanisms, the aim of actuation fatigue testing is to generate fatigue life data that can be used for the development of a life prediction design method. A potential way to use a predictive tool is to incorporate a method into the design tools and methods that are being developed to predict the response of an SMA component with the motivation of reducing the time between a concept to working component. Researchers have developed FEA models, as used in Chapter IV, to predict performance of potential SMA based actuator designs allowing for relatively accurate simulation of many potential designs before selection of a final design to be built and tested [38, 39, 41, 42]. Using the numerical mmethods reduces or even eliminates the iterative process of building, testing, and modification. Similarly, it would increase the efficiency further if these design tools had the capability to predict the actuation fatigue life. Component level fatigue testing is expensive and time consuming. A robust prediction method would help limit the necessity of fatigue testing, and eliminate fatigue testing as part of the iterative design process. However, fatigue testing is necessary to certify a design prior to commercial use, so a predictive tool reduces the necessary fatigue testing, and not eliminate it completely.

Many experimental studies have been conducted on actuation fatigue testing and two methods for life prediction have been posed [29, 30, 31, 32, 33, 34, 35]. From these works, a stress-based and a strain-based method have been presented for life prediction of actuation under constant stress [29, 31, 33]. The Wohler model was modified by replacing the cyclic stress amplitude with the applied stress, which is constant during an actuation fatigue test, in the stress-based method. The study by Bigeon and Morin (1996) showed this method to be useful for actuation fatigue tests

with complete transformation at multiple stress levels [29]. The strain-based method seen in Lagoudas et. al (2009) and Bertacchini et. al (2009) uses a reformulated version of the Mason-Coffin relation, in which the relation is integrated to compare the total plastic strain to fatigue life rather that the rate of irrecoverable strain generation. The two studies showed this method to be effective while considering a constant level of actuation, but model parameters changed with a change in the amount of actuation. A robust method for actuation fatigue life prediction has not been developed that accounts varying levels of transformation with varying stress to the author's knowledge.

A work-based method has been developed to predict actuation fatigue lives as an alternative to the stress or strain based methods found in the literature to account for varying stress levels and actuation strain and to reduce the number of necessary material parameters. This method has the potential to predict the life of a SMA actuating component based of the simulation of one duty cycle, as is done with the strain and stress based methods used for conventional metals [19]. It will be shown this method reduces to the the stress-based Wohler model shown to be effective by Bigeon and Morin (1996) if actuation strain is constant in a set of experiments [29]. The method is shown to accurately capture data with previously gathered data from Bertacchinni et. al (2009), Lagoudas et. al (2009), and Schick (2009) though more data is needed to determine the robustness of the method [31, 33, 34].

A. Work-Based Method

Many energy-based methods for fatigue life prediction have been developed for conventional metals, mainly to account for multi-axial loading [43]. In a method developed by Ellyin and Gollos (1988), the change in work density, defined as the work

being done to a material during each cycle, was correlated to fatigue life [44]. A key difference between this method and other methods posed, is that in the Ellyin and Gollos method, the complete amount of work done is considered, which is comprised of the work done to elastically and plastically deform the material in conventional metals. Considering the energy consumed by elastic deformation allows for this method to predict high cycle fatigue lives, where there is little to no energy used to plastically deform a material. This work-based method has been used to effectively predict fatigue life in high and low cycle fatigue accounting for multi-axial loading as well as non-zero mean stress cycling.

Calculating the work density amplitude is a straight forward process of integrating the stress-strain response, neglecting parts of the curve where the strain rate and stress have opposite sign, in conventional metals. In actuation fatigue experiments, the work density amplitude is simply the actuation strain multiplied by the applied stress for uniaxial, constant stress, actuation fatigue tests, as shown in eq. 5.1.

$$w_a = \varepsilon_{act}\sigma \tag{5.1}$$

σ is the applied stress, w_a is the work-density amplitude, and ε_{act} is the actuation strain. A three dimensional constitutive model would have to be utilized for more complex loading. The work-density amplitude is correlated to the fatigue life using an exponential relation, as shown in eq. 5.2.

$$w_a = A(N_f)^B \tag{5.2}$$

A and B are material parameters, w_a is the work-density amplitude, and N_f is the number of cycles to failure.

It can be shown that if the level of actuation strain remains constant, the work-

based method reduces to the stress-based, or Wohler model used by Bigeon and Morin (1996). The modified version of the Wohler model can be derived by assuming that the actuation strain constant and combining equations 5.1 and 5.2. The relation between applied stress and number of cycles to failure is shown in eq. 5.3.

$$\sigma = \frac{A}{\varepsilon_{act}}(N_f)^B \tag{5.3}$$

Similarly, a modified version of the strain-based approach commonly used in conventional metals can be derived. Using such an approach requires that the applied stress to be constant in a set of experiments. The relation between the strain amplitude and the number of cycles to failure is shown in eq. 5.4.

$$\varepsilon_{act} = \frac{A}{\sigma}(N_f)^B \tag{5.4}$$

B. Model Comparison

The data from Lagoudas et. al. (2009) was fit to a work-based curve. In this previous study, actuation fatigue tests were conducted on NiTiCu wire specimens at two applied stress, 80 MPa and 150 MPa, with varying levels of actuation. The fit of the data is shown in Fig. 33. The data was compared the to the equivalent strain-based approach using the parameters for the work-based model and eq. 5.4. The data and the resulting curves are shown in Fig. 34. It is observed that the reduction to the strain-based approach would be adequate if only one applied stress was considered.

The next study used to show the effectiveness of the work-based approach is the work of Bertacchinni et. al. (2009) [33]. The researchers conducted actuation fatigue tests in a corrosive and non-corrosive environment on wire specimens with the same composition NiTiCu as Lagoudas et. al (2009) but with a different heat treatment. The results from non-corrosive tests will be considered for the current work. In

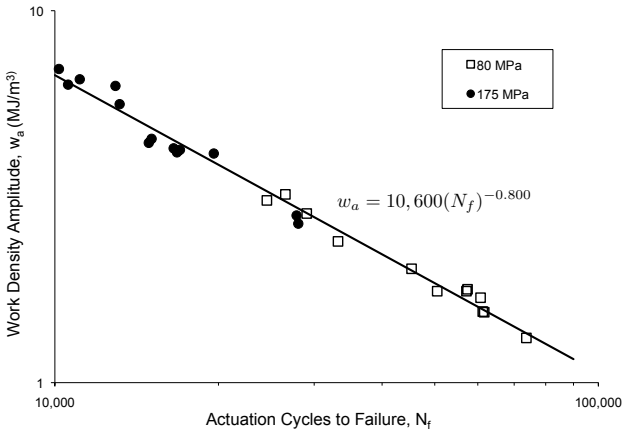

Fig. 33. Work density amplitude vs number of cycles to failure for results presented in Lagoudas et. al (2009)

Bertacchinni et. al (2009), complete actuation tests were conducted at multiple stress levels, and two partial actuation fatigue tests were conducted. A complete fit of the data to the work-based model is presented in Fig 35. Using eq. 5.3, the parameters were used to fit the data to the modified Wohler model. The data and resulting S-N curves are shown in Fig. 36.

The last study considered, was the work of Schick (2009), in which complete actuation fatigue tests were conducted at three stress levels, 100, 150 and 200 MPa, on Ni60Ti40 (wt. %) specimens. This data was originally presented in the modified Wohler model, and scatter was observed. Using the work-based method provided for a better curve fit by comparison of the coefficient of determination, which was 0.615 for the modified Wohler model and 0.689 for the work-based fit. The resulting work-life data and corresponding curve are shown in Fig. 37.

From a comparison of the resulting actuation fatigue material parameters, it can be seen that the exponent B ranges from -0.600 to -0.900. It is also observed that the heat treatment of a material will change the actuation fatigue parameters by comparing Figs. 35 and 33.

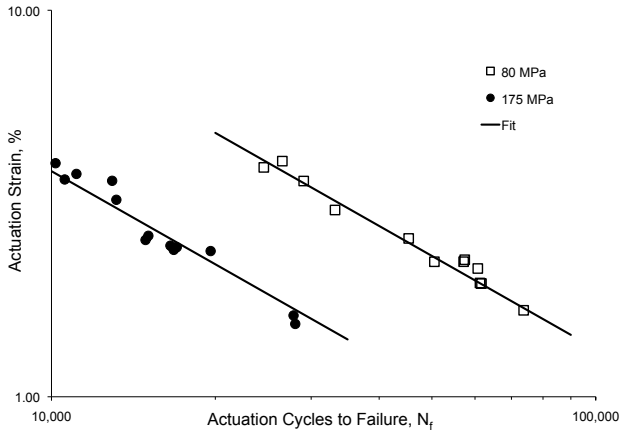

Fig. 34. Actuation strain vs number of cycles to failure for results presented in Lagoudas et. al (2009)

C. Life Prediction

Sample predictions were conducted using the data presented in Lagoudas et. al (2009) to show the effectiveness of the method [31]. The fatigue life data from tests conducted at 80 MPa was used to predict the actuation fatigue lives at 175 MPa. From the 80 MPa data, the parameter A was found to be 7030 J/cc and B was found to be -0.764. A strain life prediction was obtained by using these parameters and eq. 5.4. The data was compared with the predicted values, the results are shown in Fig. 38. It was seen that the maximum error was 21%, with the prediction being conservative. The maximum error when the prediction was greater than the observed value was 11%.

Using the results from experiments conducted at 175 MPa, the actuation fatigue lives were predicted using parameters calculated from the experiments conducted at 80 MPa to reflect the more likely scenario in a design application. Tests at 175 MPa would take less time, so if they can accurately predict tests at lower stress levels, the amount of time necessary to gather sufficient actuation fatigue life results would be drastically decreased. The parameter A was found to be 31,900 J/cc and

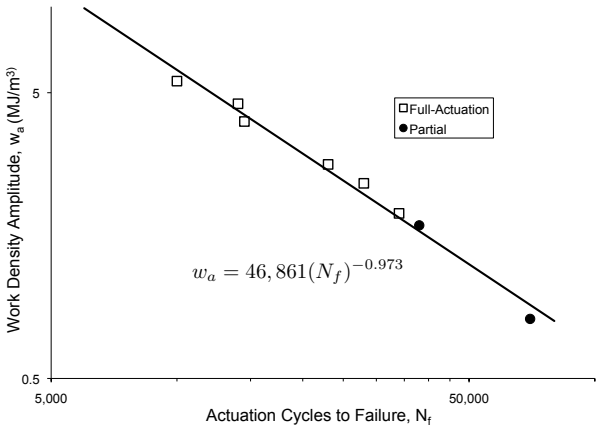

Fig. 35. Work density amplitude vs number of cycles to failure for results presented in Bertacchinni et. al (2009)

the exponent B was found to be -0.915 from least squares fitting of the fatigue life data at 175 MPa. The resulting strain-life curves are shown in Fig. 39. Testing at a high stress level is less accurate for predicting the fatigue lives at a lower stress level than using data gathered at a lower stress level at a higher stress level for this material system. However, using a higher stress level to predict fatigue lives was more conservative. It is seen that predicting from different sets of data results in different curves by comparing the fatigue parameters, indicating that large extrapolation would be inaccurate. As such, fatigue tests should be conducted at similar work-density amplitudes to predictions for a particular component design if such a method in order to use the proposed work-based method for life prediction.

D. Comments and Discussion

It was seen that the work-based method accurately captured results presented in three previous works. Actuation fatigue life results presented in Lagoudas et. al (2009), Betacchinni et. al (2009) and Schick (2009) were fit to the work-based model, and good agreement was observed. Using the results of Lagoudas et. al (2009), it was shown

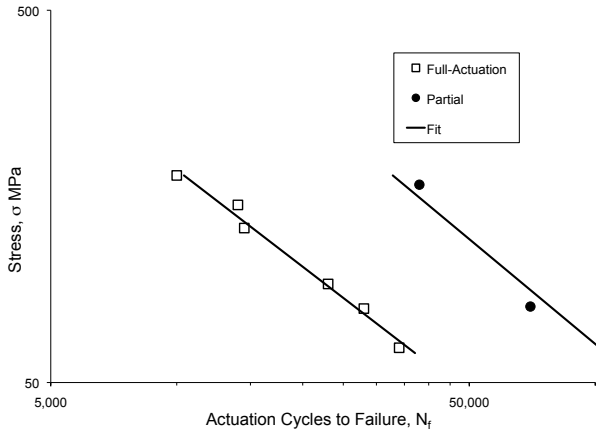

Fig. 36. Applied stress vs number of cycles to failure for results presented in Bertacchinni et. al (2009)

that the work-based method could be used to accurately predict actuation fatigue lives of tests at one stress level based off experiments conducted at another stress level. It is concluded that using actuation fatigue experiments with multiple strain amplitudes at one stress level could be used to get the actuation fatigue parameters to predict the fatigue life of tests conducted at a different applied stress level.

While these studies show the work-based method is useful for constant amplitude experiments, further studies are necessary to conclusively determine the effectiveness of such an approach to account for non-constant applied stress levels and actuation strain amplitudes. This method also has potential to predict pseudoelastic fatigue lives, but further studies would need to be conducted in which actuation and pseudoelastic fatigue experiments were conducted a single material system.

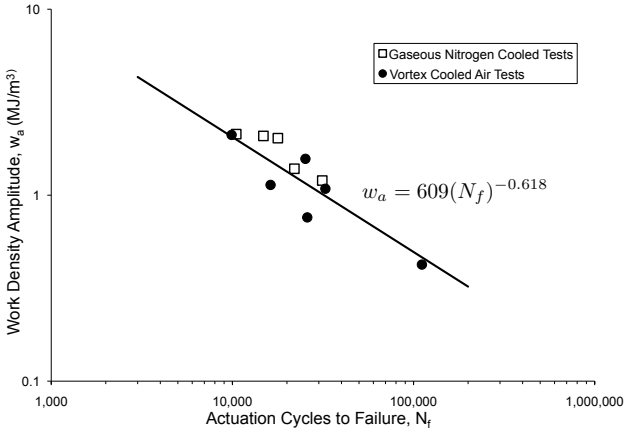

Fig. 37. Applied stress vs number of cycles to failure for results presented in Schick (2009)

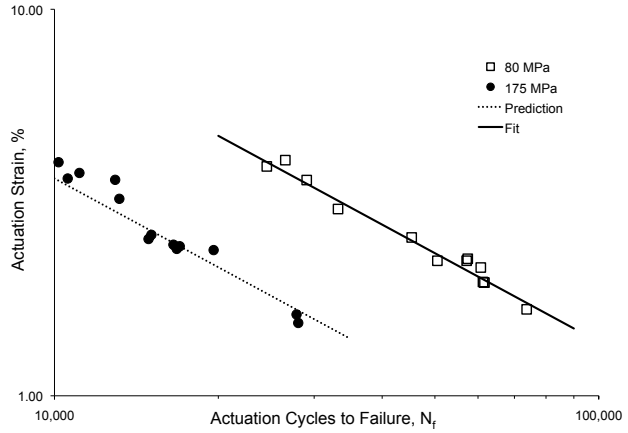

Fig. 38. Actuation strain vs number of cycles to failure data, with prediction results of tests conducted at 80 MPa using parameters calculated using results from tests conducted at 175 MPa

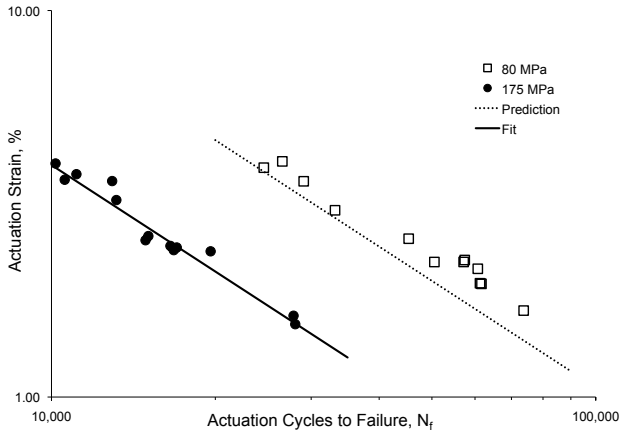

Fig. 39. Actuation strain vs number of cycles to failure data, with prediction results of tests conducted at 175 MPa using parameters calculated using results from tests conducted at 80 MPa

CHAPTER VI

CONCLUSIONS AND FUTURE WORK

A. Conclusions and Summary

Three key contributions are made to the field of actuation fatigue of SMAs in the current work. First is the development of an actuation fatigue testing method. Second is the observation of dependence of actuation fatigue life on homogenization time and orientation of Ni_3Ti precipitates in Ni-rich SMAs. Last is the work-based method, which can be used a design tool to accelerate design processes by reducing the iterative steps of build, test and modify.

1. Testing Method

The testing method in this work was shown to quickly and consistently thermally cycle SMA flat-sheet fatigue specimens under constant stress through complete actuation. Specimen geometry was chosen from a previous work, but with all dimensions doubled to reduce scatter in fatigue life results. Specimens were machined using electro-discharge machining, heat treated, with a homogenization and aging treatment, and polished prior to testing. During testing, specimens were placed in a chilled environment, maintained below the martensitic finish temperature, with a suspended weight attached. An AC current was applied to heat specimens into the austenitic phase, and removed to allow specimens to convectively cool back into the martensitic phase. The testing method allowed for observation of actuation strain and accumulation of irrecoverable strain throughout the life of specimens by utilizing an LVDT.

2. Microstructural Effects

The developed testing method presented was used to show effects of homogenization time and orientation of Ni_3Ti precipitates on actuation fatigue life of Ni60Ti40 (wt.%) SMA specimens. It was observed that increasing homogenization time increased actuation strain, accumulation of irrecoverable strain and actuation fatigue life. Another key trend observed was effects of irrecoverable strain. It was seen that actuation fatigue life increased with the amount of stabilized irrecoverable strain generation. Irrecoverable strain in Ni60Ti40 (wt.%) specimens was comprised mostly of plastic strain, rather than retained martensite and damage, as all specimens had constant actuation strain through cycling, and most irrecoverable strain was accumulated in 5-10% of transformation cycles for each specimen. Plastic strain served as mechanism to lower stress concentrations through generation of a residual stress field.

Results also showed that precipitate orientation affected actuation fatigue life and cracking behavior. It was seen that in specimens with precipitates oriented within 45^o of loading, actuation fatigue life was much greater than when precipitates were oriented greater than 45^o from the direction of loading. Postmortem analysis using optical microscopy showed cracking occurred inside precipitates oriented parallel to loading and at the interface between precipitates oriented perpendicular to loading and the transforming matrix. There was an increased number of cracks when precipitates were uniformly oriented with loading, as compared to specimens with variation in orientation of precipitates. Minimal auxiliary cracking was observed in specimens with precipites oriented perpendicular to loading. Resistance to crack growth is higher when precipitates are oriented parallel to loading, which results in higher crack densities and longer fatigue lives.

Numerical simulations were done of an elastic inclusion inside a transforming

matrix to further explain experimentally observed change in cracking behavior. A two dimensional plane stress boundary value problem was solved of an ellipsoidal inclusion with an aspect ratio varying between from 1 to 2.5 and an area fraction of 21.5% inside transforming matrix. A uniform load equivalent to 200 MPa was applied on one boundary, and temperature was lowered from above the austenitic start temperature, to below the martensitic finish temperature. Orientation and aspect ratio of precipitates were varied through multiple simulations. Results showed that stress inside precipitates increased when precipitates were aligned with loading which explains why cracking was observed inside the precipitates oriented parallel to loading in actuation fatigue tests. Results also showed a dependence of effective actuation strain on orientation of Ni_3Ti precipitates. Simulations with precipitates oriented in the loading direction had the lowest predicted effective actuation strain, and predicted effective actuation strain was greatest when precipitates were oriented perpendicular to loading.

3. Work Based Method for Actuation Fatigue Life Prediction

A work-based method for actuation fatigue life prediction was developed and shown to be effective using results from previous researchers. The work-based approach was shown to be equivalent to the stress based approach found to be effective in literature if only one level of actuation strain at multiple applied stress is considered. The work-based method was used to accurately predict actuation fatigue lives from a set of experiments conducted at one stress level with multiple actuation strain levels using parameters calculated from experiments conducted on the same material system at a different stress level with varying levels of actuation strain. The work-based method shows promise as a life predictive tool for future SMA actuator designs from these preliminary results, but at this point there is not sufficient data to conclusively

determine its robustness of such an approach.

B. Future Work

As every study generates at least as many questions as it answers, suggestions of future studies are listed below.

1. Testing Method

One extension of the testing method would be to add a way to create non-constant loads through temperature-induced transformation. A non-constant stress through transformation would more accurately capture loadings in applications like the VGC than current testing methods. Results would also be useful for validation of the work-based method or development of another actuation fatigue life prediction method. A key challenge in such an approach would be in the determination of the desired variation in stress through transformation, as this is unique for every actuator application.

Another potential for future work is to add a method for monitoring crack initiation and growth throughout thermal cycling. Tests would be paused at set intervals through cycling, and specimen surfaces would be replicated to monitor crack initiation and growth throughout fatigue life. Results would be useful for development of maintenance and inspection schedules for future actuating SMA components.

2. Microstructural Effects

One key future study is to further explore effects of homogenization time. To this end, actuation fatigue experiments should be conducted a set of specimens with varying homogenization times to observes its effect on fatigue life and generation of irrecoverable strain. The two points used in the current study are insufficient to observe

optimal homogenization time for Ni60Ti40 (wt. %) material system.

Numerical simulations of transformation induced plasticity would further explain effects of irrecoverable strain on localized stress concentrations. Simulations would show residual stress fields generated though transformation-induced plasticity, and would show a change in localized cyclic stresses with increasing irrecoverable strain. These simulations could be used to generate an optimal processing procedure for actuators prior to use in aerospace and automotive applications.

3. Work Based Approach

As previously mentioned, more testing is needed to determine robustness of the work-based method. To this end, future actuation fatigue tests should focus on different loading paths. One key variation to be considered would be partial actuation experiments, with constant actuation strain amplitudes, but with different mean volume fractions of one of the phases. Another key consideration would be non-constant strain amplitude tests, to determine if Miner's rule can be used with SMAs and the work-based method. Once the robustness of the method is defined, implementing the method into numerical design tools would be the final step.

REFERENCES

[1] W. Buehler, J. Gilfrich, R. Wiley, Effect of low-temperature phase changes on mechanical properties of alloys near composition tini, Journal of Applied Physics 34 (1963) 1475–1477.

[2] A. Pelton, D. Stockel, T. Duerig, Medical uses of nitnol, Material Science Forum 317-328 (2000) 63–70.

[3] S. Thompson, An overview of nickel-titanion alloys used in dentistry, International Endodontic Journal 33 (2000) 297–310.

[4] T. Yoneyama, H. Doi, E. Kobayashi, H. Hamanaka, Super-elastic property of tini alloys for use in dentistry, Frontiers Medical and Biological Engineering 10 (2) (2000) 97–103.

[5] D. Stockel, Shape memory actuators for automotive applications, Materials and Design 11 (6) (1990) 302–307.

[6] E. Williams, M. Elhinia, An automotive sma mirror actuator:modeling, design and experimental evaluation, Jounal of Intelligent Material Systems and Structures 19 (2008) 1425–1434.

[7] D. Hartl, D. Lagoudas, Aerospace applications of shape memory alloys, Proc. of Instituion of Mechanical Engineers, Part G, Journal of Aerospace Enginers 221 (2007) 535–552.

[8] G. Magri, M. Romagnoli, C. D. Perna, Sma actuator for gas combi boiler diverting valve, Sensors and Actuators 128 (2006) 355–366.

[9] F. Calkins, J. H. Mabe, G. Butler, Boeing's variable geometry chevron: morphing aerospace structures for jet noise reduction, Proc. of SPIE 6171 (2006) 199–210.

[10] J. Mabe, Variable area jet nozzle for noise reduction using shape memory alloy actuators, Proc. of Acoustics.

[11] L. Jordan, M. Masse, J. Collier, G. Bouquet, Effects of thermal and thermomechanical cycling on the phase transformations in niti and ni-ti-co shape memory alloys, Journal of Alloys and Compounds 211/212 (1994) 204–207.

[12] P. McCormick, Y. Liu, Thermodynamic analysis of the martensitic transformation in niti-ii. effect of transformation cycling, Acta Metalurgica an Materialia 42 (1994) 2407–2413.

[13] S. Miyazaki, T. Imai, Y. Igo, K. Otsuka, Effect of cyclic deformation on the psuedoelasticity characteristics of ti-ni alloys, Metallurgical Transactions A 17A (1986) 115–120.

[14] B. Strnadel, S. Ohashi, T. I. H. Ohtsuka, S. Miyazaki, Cyclic stress-strain characteristics of ti-ni and ti-ni-cu shape memory alloys, Material Science and Engineering A 202 (1995) 148–156.

[15] A. Pelton, V. Schroeder, M. Mitchell, X. Gong, M. Barney, S. Robertson, Fatigue and durability if nitinol stents, Journal of the Mechanical Behavior of Biomedical Materials 1 (2008) 153–164.

[16] L. Delaey, J. Janssen, D. V. de Mosselaer, G. Dullenkopf, A. Deruyttere, Fatigue properties of psuedoelastic cu-zn-al alloys, Acta Materialia 12 (1978) 373–376.

[17] K. Melton, O. Mercier, Fatigue life of cuznal alloys, Scripta Metallurgica 13 (1979) 73–75.

[18] K. Melton, O. Mercier, Fatigue of niti thermoelastic martensites, Acta Metalurgica 27 (1979) 137–144.

[19] N. Dowling, Mechanical behavior of materials: engineering methods for deformation, fracture and fatigue, Pearson Prentice Hall, Upper Saddle River, NJ, 2007.

[20] A. M. Figueiredo, P. Modenesi, V. Buono, Low-cycle fatigue life of superelastic niti wires, International Journal of Fatigue 31 (2009) 751–758.

[21] Y. Furuichi, H. Tobushi, T. Ikawa, R. Matsui (Eds.), Fatigue properties of a TiNi shape memory alloy wire subjected to b, Vol. 217, Instituion of Mechanical Engineers Part L Journal of Materials Design and Applications, Professional Engineering, 2003.

[22] N. Siredey-Schwaller, A. Eberhardt, P. Bastie, Parameters influencing the fatigue of life of a cu-al-be single-crystal shape memroy alloy under repeated loading, Smart Materials and Structures 18 (2009) 1–8.

[23] H. Tobushi, T. Nakahara, Y. Shimeno, T. Hashimoto, Low-cycle fatigue of tini shape memory alloy and formulation of fatigue life, Journal of Engineering Materials and Techology 122 (2000) 186–191.

[24] M. Wagner, G. Eggeler, New aspects of bending rotation fatigue in ultra-fine-grained psuedo-elastic niti wires, International Journal of Material Res. 97 (2006) 1687–1696.

[25] K. Wilkes, P. Liaw, The fatigue behavior of shape-memory alloys, Journal of Materials (2000) 45–51.

[26] A. Mckelvey, R. Ritchie, Fatigue-crack growth behavior in the superelastic and shape-memory alloy nitinol, Metallurgical and Materials Transactions A 32A (2001) 731–743.

[27] J. McNichols, P. Brookes, Niti fatigue behavior, Journal of Applied Physics 52 (12) (1981) 7442–7444.

[28] K. Melton, O. Mercier, The effect of the martensitic phase transformation on the low cycle fatigue behaviour of polycrstalline ni-ti and cu-zn-al alloys, Material Science and Engineering 40 (1979) 81–87.

[29] M. Bigeon, M. Morin, Thermomechanical study of the stress assisted two way memory effect fatigue in tini and cuznal wires, Scripta Materialia 35 (12) (1996) 1373–1378.

[30] D. Miller, Thermomechanical characterization of plastic deformation and transformation fatigue in shape memory alloys, Ph.D. thesis, Texas A & M University (2000).

[31] D. Lagoudas, D. Miller, L. Rong, P. Kumar, Thermomechanical fatigue of shape memory alloys, Smart Materials and Structures 18 (2009) 1–12.

[32] O. Bertacchini, Characterization and modeling of transformation induced fatigue of shape memory allloy actuators, Ph.D. thesis, Texas A & M University (2009).

[33] O. Bertacchini, D. Lagoudas, E. Patoor, Thermomechanical transformation fatigue of tinicu sma actuators under a corrosive environment-part i: Experimental results, International Journal of Fatigue 31 (2009) 1571–1578.

[34] J. Schick, Transformation induced fatigue of ni-rich niti shape memory alloy actuators, Master's thesis, Texas A & M University (2009).

[35] K. Ramaia, C. Saikrishna, V. Ranganath, S. Bhaumik, Fracture of thermally activated niti shape memory alloy wires, Material Science and Engineering A 528 (2011) 5502–5510.

[36] ASTM, ASTM Standard Practice for Strain-controlled Fatigue Testing, ASTM International, West Conshocke, PA, 2006.

[37] J. Boyd, D. Lagoudas, A thermodynamical constitutive model for shape memory materials. part i. the monolithic shape memory alloy, International Journal of Plasticity 12 (1996) 805–842.

[38] M. A. Qidwai, D. Lagoudas, Numerical implementation of a shape memory alloy thermomechanical constitutive model using return mapping algorithms, International Journal for Numerical Methods in Engineering 47 (2000) 1123–1168.

[39] D. Hartl, D. Lagoudas, F. Calkins, Advanced methods for the analysis, design and optimization of sma-based aerostructures, Smart Materials and Structures 20 (2011) 1–20.

[40] Abaqus, Analysis User's Manual, Dassuult Systems of America Corp., Woodland Hills, CA (2009).

[41] M. Panico, L. Brinson, A three-dimensional phenomenological model for martensite reorientation in shape memory alloys, Journal of the Mechanics and Physics of Solids 55 (2007) 2491–2511.

[42] F. Auricchio, R. Taylor, Shape-memory alloys: modeling and numerical simulations of finite-strain superelastic behavior, Comput Methods Appl. Mech. and Engrg. 143 (1997) 175–194.

[43] D. Socie, G. Marquis, Multiaxial Fatigue, SAE International, Warrendale, PA, 2000.

[44] F. Ellyin, K. Golos, Multiaxial fatigue damage criterion, Journal of Engineering Materials and Techology 110 (1988) 63–68.

VITA

Chris Calhoun is the youngest of two sons. He was born and raised in Reno, NV. He attended Galen High School in Reno. He went on to attend Virginia Polytechnic Institute and State University, where he obtained a Bachelor of Science in engineering science and mechanics in May of 2009. Upon graduation Chris moved his studies to College Station, TX, where graduated with his Master of Science in aerospace engineering in May of 2012 from Texas A&M. After graduation, he will pursue a PhD at the University of Virginia in Material Science and Engineering. A full resume can be found at http://smart.tamu.edu.

Aerospace Engineering
c/o Dr. Dimitris Lagoudas
Texas A&M Unversity College Station, TX 77843-3141
His email address is cacalhou@tamu.edu.